Strål
säkerhets
myndigheten
Swedish Radiation Safety Authority

Research

Stress field modelling of the Forsmark lens – Correlation of stress measurements with stress field simulations

2024:01

Author: Daniel Bücken, Livia Nardini and Tobias Meier
Geomecon GmbH. Reuchlinstraße 10. 10553 Berlin. Germany
Date: January 2024
Report number: 2024:01
ISSN: 2000-0456
Available at www.ssm.se

Strål
säkerhets
myndigheten
Swedish Radiation Safety Authority

Author: Daniel Bücken, Livia Nardini and Tobias Meier
Geomecon GmbH. Reuchlinstraße 10. 10553 Berlin. Germany

2024:01

Stress field modelling of the Forsmark lens – Correlation of stress measurements with stress field simulations

Date: January 2024
Report number: 2024:01
ISSN: 2000-0456
Available at www.stralsakerhetsmyndigheten.se

SSM perspective

Background and objective

Understanding the in-situ stress field in the Forsmark tectonic lens will lay the fundamental basis to characterise the prevailing mechanical and hydraulic behaviour of the rock mass. Only with a good understanding of the geomechanical setting including the stress field an analysis of future rock mass behaviour under the evolution of conditions in a repository for spent nuclear fuel is possible. Based on the existing stress measurements several stress models have been published. The stress model frequently used by SKB (Martin, 2007), mostly ignores hydraulic measurements, and proposes a reverse faulting regime. An alternative stress model (Ask et al. 2007) heavily relies on the hydraulic data and suggests a strike slip stress model with smaller stress magnitudes. A recent review by Gipper et al. (2015), incorporating most measurements, suggests a model in the hybrid regime. In order to get a better understanding of the stress situation of the Forsmark area and to gain more confidence in the analyses, a comprehensive stress modelling and simulation study was performed on the Forsmark lens taking into account existing stress measurements and large brittle structures.

Results

The numerical model developed is the result of an integrated study based on the elaboration of geomechanical concepts applied to a structurally complex rock mass. The input data for the model included the geometrical elements that characterise the region of interest at the km scale (i.e. the fault network), measurement data collected over various campaigns for the determination of the in-situ state of stress, experimentally derived values for the main geomechanical properties of the rock mass as well as the interpretations of said measured and derived parameters formulated at different stages of the site characterisation process.

The complexity of the structural elements and the high variability of many of the input parameters and data collected in the area generated uncertainties in the resulting numerical model. While it is difficult to quantify the accumulated uncertainty in the material parameters, generated by all the mentioned uncertainties, it is reasonable to suggest that the overall heterogeneity of the rock volume could be at least partially underestimated. As mentioned, local (at times considerable) heterogeneities are recognised within and around deformation zones; given the complexity of the tectonometamorphic evolution of the area, as well as the relative lithological variations within the region of interest, further sources of uncertainty could have been overlooked and not properly sampled.

As a result, the proposed model is characterised by an orthotropic material behaviour for the rock volume, where the increase of the Young's modulus with depth is different in the directions parallel and perpendicular to the major principal stress. While the testing conducted on intact rock core samples does not support this hypothesis, strongly converging SH and Sh gradients with depth as proposed by Martin (2007), cannot be reproduced for a completely isotropic body. The choice is further justified by the mentioned sampling bias, which could have overlooked the effect of preferentially oriented sets of fractures and other structures on the overall material behaviour of the rock volume as a whole.

However, in the absence of better quality (and less variable) stress measurements, our modelling cannot reduce the risk that none of the originally proposed models for the Forsmark site (neither Martin, 2007 nor Ask et al., 2007) is in fact a realistic representation of the actual in-situ stress in the area.

Conclusions

Discrete faults seem to play a minor role in the current stress field in contrast to the spatial and heterogeneous distribution of rock properties. Research should be conducted on the spatial distribution and the range of rock properties so that calibrated distribution functions can be derived to populate the subsurface not with constant rock property values but with distribution functions that are based on spatial information or calibration. This might better address the uncertainties in the measured stresses than trying to approximate homogenized gradients not accurately describing the scatter of measured values. The performed modeling highlights the influence of elastic parameters on the stress field and shows how an assumption of a heterogeneous Young's modulus and Poisson's ratio of ±10% could describe the spread in the range of the most-likely stress field.

Hence, upcoming work could improve the capabilities of the model by deriving spatial distribution function of elastic properties that are calibrated against the stress field measurements.

Project information

Contact person SSM: Carl-Henrik Pettersson
Reference: SSM2018-3018/ 3030045-46

SSM perspektiv

Bakgrund och syfte

Kunskap om det nuvarande bergspänningsfältet i Forsmark ligger till grund för att karakterisera bergmassans rådande mekaniska och hydrauliska beteende. Endast med en god förståelse för den geomekaniska miljön är en analys av bergmassan framtida hydro-mekaniska beteende möjlig. Baserat på befintliga bergspänningsmätningar har flera modeller tagits fram. Den bergspänningsmodell som ofta används av SKB (Martin, 2007) baseras huvudsakligen på bergspänningsmätningarna ner till 500 m djup med överborrningsmetoden och föreslår en revers förkastningsregim. Dessa mätningar exkluderar tidigare bergspänningsmätningar på förvarsdjup utförda med den hydrauliska spräckningsmetoden och hydraulisk provning av redan existerande sprickor. En alternativ spänningsmodell (Ask et al. 2007) förlitar sig till stor del på de hydrauliska mätningarna och föreslår en strike-slip modell med mindre spänningsmagnituder. En studie av Gipper et al. (2015), som omfattar huvuddelen av bergspänningsmätningarna, föreslår en hybridmodell där reversa spänningsförhållanden övergår till strike-slip med ökat djup. För att få en bättre förståelse av bergspänningssituationen i Forsmarksområdet, och för att få mer förtroende för analyserna. genomfördes en omfattande spänningsmodellering och simuleringsstudie på Forsmarkslinsen med hänsyn till befintliga bergspänningsmätningar och den rumsliga fördelningen av kilometerstora förkastningar.

Resultat

Den numeriska modellen baseras på den rumsliga fördelningen av kilometerstora förkastningar runt det planerade slutförvaret för använt kärnbränsle i Forsmark, bergspänningsmätningar samt bergmassans bergmekaniska egenskaper erhållna från laboratorieexperiment. Svårigheten att modellera förkastningarna rumsliga fördelning i bergmassan och bergspänningsmätningarnas höga variabilitet genererade osäkerheter i den numeriska modellen. Heterogeniteter inom och runt deformationszoner och bergmassan i övrigt kan vara ytterligare källor till osäkerhet som inte beaktats i tillräckligt stor utsträckning vid bergspänningsmätningarna.

Den föreslagna modellen karakteriseras av ett ortotropiskt beteende, där ökningen av Youngs modul med djupet är olika i riktningarna parallella och vinkelräta mot huvudspänningen. Även om de tester som utförts på intakta borrkärnprover inte stöder denna hypotes, kan starkt konvergerande SH- och Sh-gradienter med djup som föreslagits av Martin (2007) inte reproduceras för en helt isotrop bergmassa. Valet motiveras ytterligare av potentiell provtagningsbias, vilket kan förbise i vilken utsträckning spröda strukturers dominerande orientering påverkar bergmassas mekaniska beteende.

I avsaknad av ytterligare spänningsmätningar kan den utförda modelleringen inte avgöra vilken av de föreslagna bergspänningsmodellerna för Forsmark är den mest realistiska representationen av bergspänningsförhållandena i Forsmark.

Slutsatser

Förkastningar kan spela en mindre roll för bergspänningsfältets variabilitet jämfört med den rumsliga variabiliteten i bergmassans egenskaper. Forskning bör därför inriktas på den rumsliga fördelningen av bergmassans egenskaper samt dessas spännvidd. Information som kan ligga till grund en parametrisering av bergmassans mekaniska egenskaper med fördelningsfunktioner snarare än konstanta värden. Ett tillvägagångssätt som har potential att bättre hantera osäkerheterna i de uppmätta bergspänningarna än att försöka approximera homogeniserade gradienter som inte exakt beskriver spridningen av uppmätta värden.

Den utförda modelleringen belyser inverkan av elastiska parametrar på spänningsfältet och visar hur ett antagande om en heterogen Youngs modul och Poissons kvot på ±10 % skulle kunna beskriva variabiliteten för det SKB kallar det mest sannolika spänningsfältet (Martin, 2007). En rumslig fördelningsfunktion av elastiska egenskaper kalibrerade mot bergspänningsmätningarna bedöms därför kunna förbättra bergspänningsmodellen.

Projekt information
Kontakt person SSM: Carl-Henrik Pettersson
Referens: SSM2018-3018/ 3030045-46

Stress field modelling of the Forsmark lens -

Correlation of stress measurements with stress field simulations

Daniel Bücken, Livia Nardini, and Tobias Meier

geomecon GmbH. Reuchlinstraße 10. 10553 Berlin. Germany.

Sammanfattning

Den numeriska modellen kan reproducera bergspänningsfältet som föreslagits av Martin (2007) genom att använda anisotropa, djupberoende Youngs moduler och anisotropa förskjutningsvillkor. En första ordningens approximation av spänningsmätningarna med överborrningsmetoden uppnås därför. Eftersom Martin (2007) har uteslutit data från hydrauliska bergspänningsmätningar, var reproducering av dem inte ett mål med vår modell.

Den beskrivna numeriska modellen kan dock inte reproducera spridningen i spänningsmätningar, vilket antogs kunna förklaras som spänningsförändringar nära större förkastningszoner. För att testa denna hypotes kördes parametriska svep som varierar styvheten hos de förkastningar som korsskärs av mätborrhål. Medan mindre variationer i spänningar i närheten av dessa förkastningar har observerats i den numeriska modellen (t.ex. figur 19), kan den övergripande variabiliteten inte förklaras av realistiska variationer i förkastningens bergmekaniska egenskaper. Som framgår av kapitel 8.2 skulle dock spänningsförändringarna också kunna relateras till heterogeniteter i bergdomänerna, vilket framgår av variationerna i uppmätta materialegenskaper (se figur 21).

Sammanfattningsvis kan den observerade variabiliteten i de spänningsmätningar som utförts i Forsmarksområdet inte enbart förklaras av spänningsförändringar i förkastningarnas närhet, utan tycks snarare vara resultatet av heterogeniteter i bergmassans elastiska materialegenskaper, eller en kombination av de två effekterna.

Summary

The described numerical model is successful in reproducing the stress field proposed by Martin (2007) by using anisotropic, depth-dependent Young's moduli and anisotropic displacement boundaries. A first order approximation of the overcoring stress measurements is therefore achieved. Since Martin (2007) has excluded hydraulic fracturing stress measurements, reproducing them was not a goal of our model.

The described numerical model is however unable to reproduce the spread in stress measurements, which was thought to be induced by stress alterations close to fault zones. In order to test this hypothesis we run parametric sweeps varying the stiffnesses of the faults that were cross-cut by measurement boreholes. While minor variations in stress in close proximity to these faults have been observed in the numerical model (e.g. Figure 19), the overall variability cannot be explained by realistic variations in the fracture zone parameters. As shown in Chapter 7.2, however, the stress alterations could also be related to heterogeneities in the rock domains as indicated by the variations in measured material properties (see Figure 21).

To conclude, the variability observed in the stress measurements carried out in the Forsmark area cannot be solely explained by stress alterations in the proximity of fractures zones, but rather appears to be the result of heterogeneities in the elastic material properties of the rock mass, or a combination of the two effects.

Contents

1 Introduction

In a crystalline repository setting, the mechanical and hydrogeological behaviour of the fracture network is to a large extent controlled by the acting stress field. Thus, the assessment of present- and post-closure flow rates is highly dependent on the understanding of the present stress regime, how it varies and how it can change during a glacial cycle. The stress field also provides the basis for assessing the potential for reactivation of brittle structures in the repository volume due to a distal earthquake. Therefore, in assessment of the long term safety it is of the utmost importance to understand the present stress field in a repository for spent nuclear fuel and how it might change over time.

The stress field at Forsmark is still a matter of debate as several contradicting hydraulic and overcoring stress measurements were collected in the area alongside with indications of the stress field orientation from borehole breakouts (Figure 1). Geomecon performed an integrated structural geology and geomechanical study using modern numerical tools to gain further understanding of the stress field in the Forsmark lens.

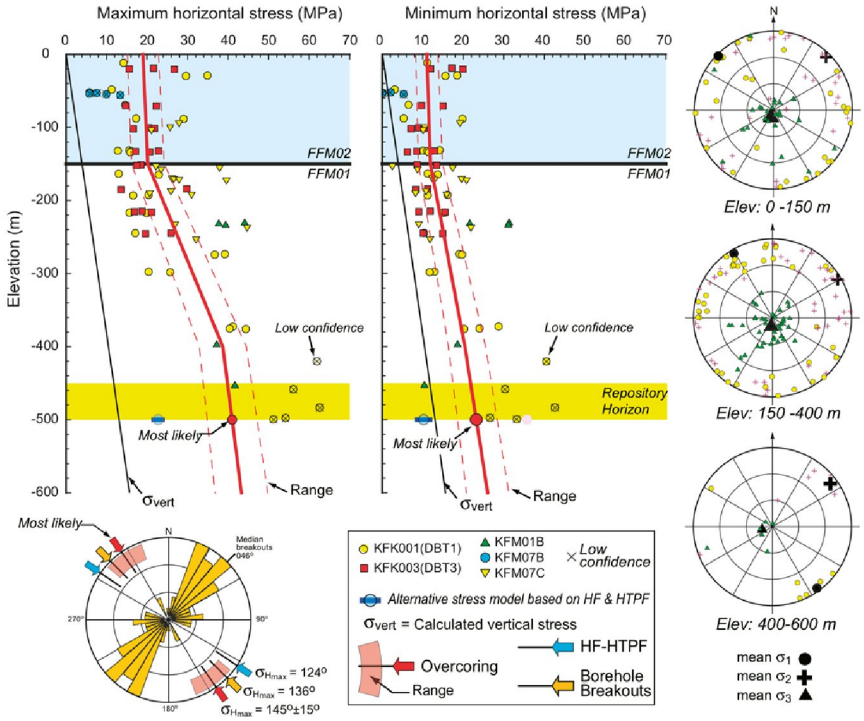

Figure 1 Stress measurement data in the Forsmark area for fracture domains FFM01 and FFM02 (from SKB TR-10-52, p.293, Figure 6-48).

Understanding the in-situ stress field in the Forsmark tectonic lens (see Glamheden et al. 2007b for further information) will lay the fundamental basis to characterise the prevailing mechanical and hydraulic behaviour of the rock mass.

Based on the existing stress measurements several stress models have been published (Table 1). The stress model referred to as "most likely" by SKB (Martin, 2007) mostly ignores hydraulic measurements, and proposes a reverse faulting regime. An alternative stress model (Ask et al., 2007) heavily relies on the hydraulic data and suggests a reverse faulting regime transitioning to strike-slip at depth, with smaller stress magnitudes. A more recent review by Gipper et al. (2015), incorporating most measurements, suggests a model in the hybrid regime.

As concluded in a previous study by Backers et al. (2014), the stress field model proposed by SKB (Martin, 2007) is unlikely from a structural-geomechanical perspective. In the study, the available data on the stress field and additional structural geology-based approaches were reviewed and it was found that there are some inconsistencies with strength parameters of the rock mass provided by SKB. Re-evaluating the available stress related data in combination with additional calculations of possible stress field scenarios may lead to the proposal of an alternative stress model. For the purpose of this analysis, the reference stress model adopted is the Martin (2007). The reasoning behind this choice is laid out in Chapter 3.1.

Table 1. Selected published stress models for the Forsmark lens at repository depth (i.e. 500 m).

SH MPa	Sh MPa	Sv MPa	PP MPa	Reference
41.0 ± 6.2	23.2 ± 4.6	13.3 ± 0.3	5	Martin (2007, R-07-26)
22.7 ± 1.1	10.2 ± 1.6	13.3	5	Ask et al. (2007, P-07-206)
35.5 ± 5	13.3 ± 2	13.3	5	Gipper et al. (2015)
56 ± 6	35 ± 15	13.3 ± 0.3	5	SKB unlikely maximum

In order to get a better understanding of the stress situation of the Forsmark area and to gain more confidence in the analyses based on stress data, a comprehensive stress modelling and simulation study based on the Finite Element Method called COMSOL Multiphysics of the Forsmark lens was performed, taking into account the existing stress measurements and the large scale structural features like deformation zones that might result in localized stress field perturbations explaining the scatter in the stress measurements.

The study is composed of the following work packages:

- WP1 - Subsurface modelling: Import of the provided structural data into COMSOL Multiphysics.
- WP2 - Data Review: Summary of the available measurement data, and implementation of monitoring points into the numerical model for later comparison.
- WP3 - Numerical modelling: Application of boundary conditions on the subsurface geological model into COMSOL Multiphysics.
- WP4 - Stress inversion: Simulation with a set of stress models, extraction and comparison of stresses to the field data.
- WP5 - Stress validation: Fine tuning of the stress conditions for verification.
- WP6. Discussion and Summary, Reporting.

The following data were provided by the Swedish nuclear fuel and waste management company (SKB):

- Stress measurement data
  - Hydraulic test data in RTF, LOG, TXT, XLSX format
  - Overcoring data in RTF, LOG, TXT, XLSX format
- Geometric model data Forsmark
  - FDZ local model -fracture zones in DGN, DWG, DXF format

- FDZ regional model _fracture zones in BAK, DGN, DWG, DXF format
- FFD fracture domains in DGN, DWG, DXF format
- Forsmark boreholes in DGN, DXF format
- Forsmark layout in DGN, DXF, PDF format
- FRD local rock domains in DGN, DXF format
- FRD regional rock domains in DGN, DXF format

> Multitude of reports and literature (not further elaborated here)

The data were used without further questioning of validity.

2 WP1 – Subsurface modelling

Converting the geometric data obtained into a numerically solvable subsurface model proved to be extremely difficult. The Finite Element Method (FEM) approach used by COMSOL Multiphysics requires a finely discretised, watertight, and well-defined geometrical model with low tolerances. The tolerances needed for successful FEM calculations are tighter than the tolerances in the provided CAD file formats; thus, a reworking of the geometry was needed.

After checking the multitude of provided geometry files in different formats, the geometry of our subsurface model was finally based on the DWG-format data from the "*Fracture Zones Regional"* dataset provided by SKB (*DZ_PFM_REG_v22.02 without boundary.dwg;* Figure 2). Other datasets proved to be unreadable, faulty, or unfit for purpose. The final fracture zone data were imported into Computer Aided Design (CAD) programs and converted into an STL-format mesh file. Using the software packages MeshLab and Meshmixer the resulting mesh was repaired and optimised. This included, among others, the removal of duplicate vertices and faces, the repair of non-manifold vertices, the repair of self-intersecting faces, the correction of mismatched borders, and the healing of holes in the fracture surfaces. Typical time-consuming mesh issues are shown in Figure 3.

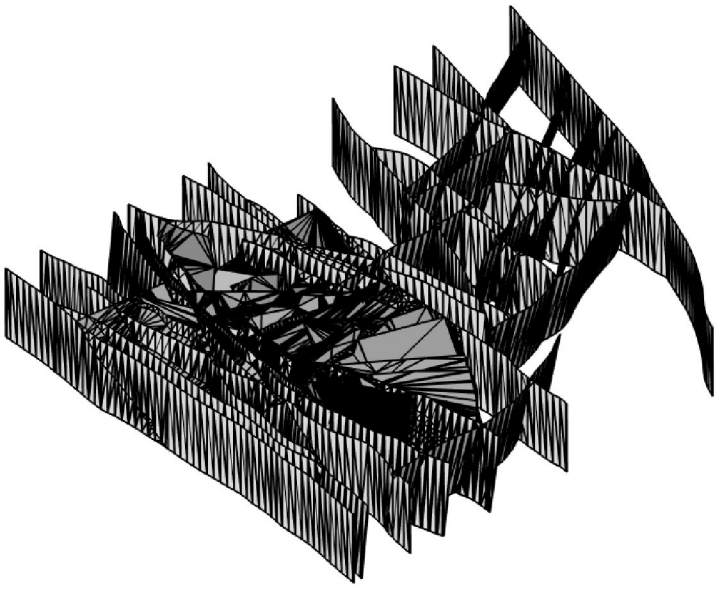

Figure 2 "Regional Fracture Zone" dataset used to create the subsurface model of this study, DZ_PFM_REG_v22.02 without boundary.dwg.

Finally, the reworked STL-file was imported into COMSOL Multiphysics and finalised into an FEM-compatible, low-tolerance, watertight geometry. The geometry was translated from its geographical coordinates to the coordinate system origin to allow for lower relative geometrical tolerances. The faults and fault zones were surrounded by a confining box which is oriented such that the orientation of the stress field as derived by Martin (2007) could be directly applied.

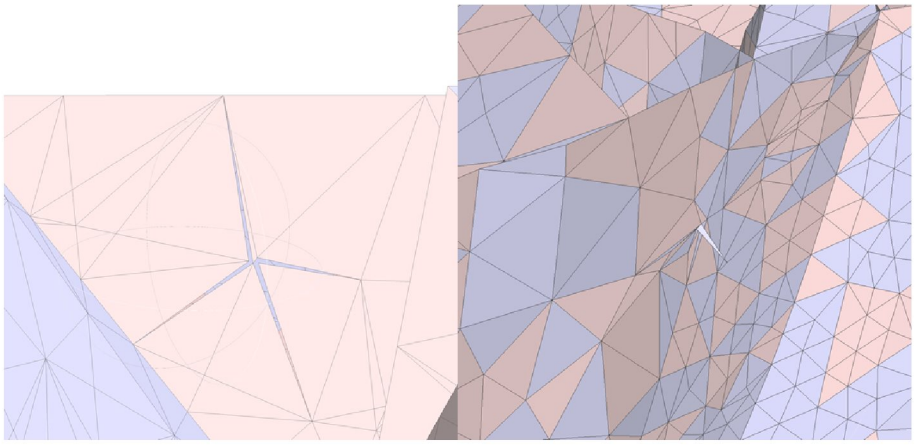

Figure 3 Typical mesh issues which had to be resolved. Left: holes in surfaces, leading to a non-watertight mesh. Right: faulty, protruding mesh-elements causing mismatching of surface intersections.

In a first step, only the subvertical fracture zones were implemented in the model (Figure 4). After their effect was characterised, a subset of the sub-horizontal fracture zones was added to the model. As not all sub-horizontal fracture zones could be implemented in the model, focus was set on fracture zones being transected by stress measurement boreholes. Figure 5 highlights the sub-horizontal surfaces incorporated in the final underground model, as well as the stress measurement locations in the boreholes KFK001_DBT1, KFM01A, KFM04A, KFM07A, KFM07C, KFM08A, KFM09A, KFM09B, KFMB01B, and KFMB02A.

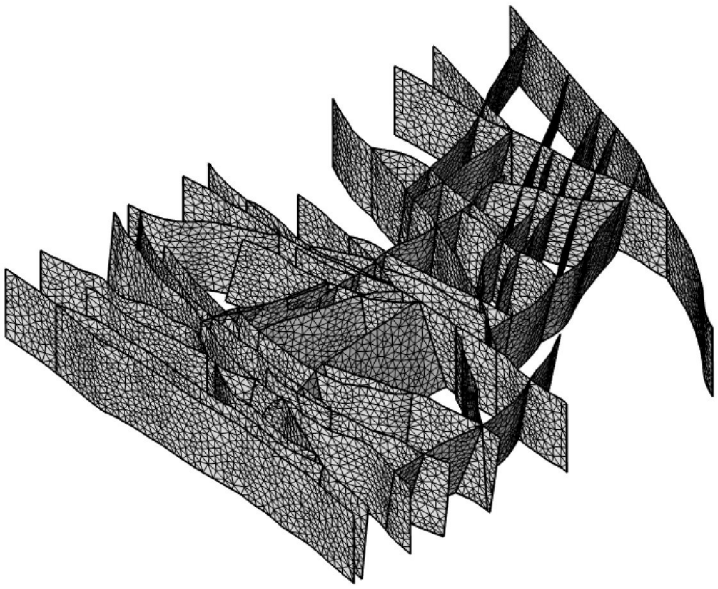

Figure 4 Thoroughly reworked mesh of the subvertical fracture zones in COMSOL Multiphysics.

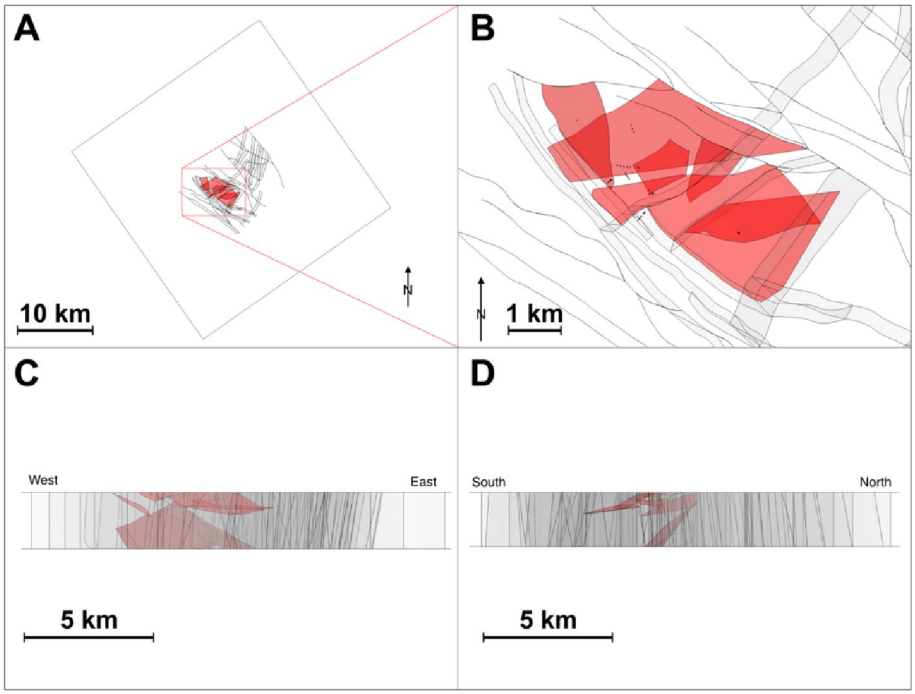

Figure 5 A) Overview of the numerical model with subvertical fracture zones in light grey, sub-horizontal fracture zones in red and the outline of the numerical model. B) Zoomed-in top view of the main area of interest in A, with the addition of the stress measurement locations. C) Side view of the numerical model, looking North. D) Side view of the numerical model, looking West.

3 WP2 – Data review

In this Chapter the input and reference data for the numerical model are reviewed.

3.1 In-situ stress field models

As mentioned in Chapter 1, several different stress field models have been proposed for the Forsmark area over the years. All models are based on the stress measurement campaigns that were conducted at the Forsmark site between the early 1980s and 2007, primarily employing overcoring and/or hydraulic fracturing (including hydraulic testing of pre-existing fractures, HTPF) techniques. The measured stress magnitudes (as well as the calculated gradients) vary greatly depending on the measurement technique adopted, on top of presenting significant variabilities within datasets. The latter are interpreted by the authors as resulting from either difficulties in carrying out the measurements (e.g. core disking below certain depths during overcoring, or sealing of pre-existing fractures preventing successful hydraulic testing) or from the intrinsic unreliability of the technique given the local stress field: as a result, the two most widely cited models (Martin, 2007, or SKB R-07-26 and Ask et al., 2007, or SKB P-07-206) are based predominantly on overcoring measurements or hydraulic stress measurements. The proposed stress gradients and stress magnitudes for both the minimum and maximum horizontal stress are substantially different in the two models, resulting in different suggested stress regimes (reverse for Martin, 2007 and reverse transitioning to strike-slip at depth for Ask et al., 2007). A review of the two stress models was commissioned by SKB to an external consultant in 2014 and furthermore resulted in the publication of an alternative (intermediate) stress model for the area (Gipper et al., 2015).

The stress magnitudes proposed at repository depth (i.e. 500 m) by the models currently published for the Forsmark area are summarised in Table 1.

For the purpose of this analysis, the reference stress model adopted is Martin (2007), also referred to as the "most likely" model by SKB. The reasons for this choice are manyfold. On top of representing a conservative estimate of the in-situ stress field, the model from Martin (2007) offers an estimate of stress gradients from surface to 600 m (with a suggested extrapolation down to 1'000 m) rather than only proposing magnitude values for the depth interval in which the repository will be located (i.e. 400 m to 600 m depth). The author also brings forward important critical aspects of the hydraulic testing stress measurement campaigns, which suggest that the use of these data for stress calculations could lead to significant errors (e.g. because hydraulic fracturing forms normal to the minimum stress, in a reverse faulting regime, the measured stress will correspond to the overburden weight).

While we are aware that some ambiguities are present in the Martin (2007) model as well (e.g. the change in slope for S_H occurring at 400 m depth is poorly justified from a geological point of view, and is inexplicably not proposed for S_h), we consider a conservative approach to be the most sensible to evaluate the behaviour of the rock mass under the varying conditions that a repository of spent nuclear fuel can undergo during its lifetime.

The chosen stress field can in any case be considered as a background stress field, which will be locally altered by the presence of fracture zones.

3.2 Geomechanical parameters

Site characterisation carried out by SKB at Forsmark included advanced multidisciplinary evaluations of the suitability to host a repository for spent nuclear fuel. The rock mechanical modelling that was conducted at different stages of the

site characterisation provides a complete evaluation of the geomechanical parameters of the rock mass in the Forsmark area, as well as a discussion over their heterogeneity as a result of local lithological and structural variations.

In particular, Glamheden et al. (2007b) (modelling stage 2.2) and Glamheden et al. (2008) (modelling stage 2.3) present detailed evaluations (based on experimental results as well as numerical modelling) of rock mechanics properties of both intact and fractured rock domains, and of the mechanical characterisation of deformation zones.

In stage 2.2 (Glamheden et al., 2007b) mechanical properties were determined for both intact rock and natural fractures, using the following testing methods:

- Uniaxial compressive test,
- Triaxial compressive test,
- Indirect tensile test,
- P-wave velocity on core samples and
- Direct tensile test

for the intact rock samples and

- Tilt test,
- Shear test

on samples containing natural fractures (both open and sealed). For the details concerning sample selection criteria and test reproducibility strategies, the reader is referred to the original report, Glamheden et al., 2007b.

3.2.1 Mechanical properties of intact rock

Intact rock samples were collected within rock domains RFM029 and RFM045 (the target volume for the repository) as well as in adjacent rock domains RFM034 and RFM017. A rock domain is intended as a homogeneous volume of rock in which the overall composition, grain size and degree of deformation are similar. Within rock domains, slight lithological differences indicate different rock types (e.g. "Granodiorite, metamorphic" or "Pegmatite, pegmatitic granite"; see Section 1.9.3 in Glamheden et al., 2007b for a full classification of rock types) which are indicated by serial numbers (in the form of 1010XX, where the last two digits are rock type-specific).

A summary of the deformation properties in the aforementioned (intact) rock domains are presented in Table 2. In Table 2, E and ν are the Young's modulus and Poisson's ratio, respectively. Strength properties were neglected here since only linear elastic material behaviour is assumed in the rock mass.

Table 2. Mean intact rock mechanical properties from Site characterisation stage 2.2 for rock domains RFM029, RFM034 and RFM017 (within the target volume for the construction of the repository and adjacent to it). After Glamheden et al. (2007b).

Rock domain	Rock type	E [GPa]	ν
RFM029	101057	78 ± 3[1]	0.24 ± 0.03
RFM034	101057	73 ± 2	0.27 ± 0.02
RFM029	101061	76 ± 3	0.30 ± 0.03
RFM034	101061	72 ± 1	0.26 ± 0.10
RFM029	101054	70 ± 3	0.29 ± 0.04
RFM017	101054	72 ± 4	0.25 ± 0.03
RFM045	101058	83 ± 3	0.27 ± 0.03

[1]Note that the uncertainty is defined as "uncertainty of the mean", quantified for a 95% confidence interval.

In stage 2.3, similar laboratory tests were carried out on new sampled material belonging to fracture domains FFM01, FFM02 and FFM06 (fracture domains are volumes of rock characterised by a similar fracture frequency; they can be sub-units of rock domains), within the target volume of the repository. The results of these investigations can be found in Table 3.

Table 3 Mean intact rock mechanical properties from site characterisation stage 2.3 for fracture domains FFM01, FFM02 and FFM06 (within the target volume for the construction of the repository). After Glamheden et al. (2008).

Fracture domain	Rock type	E [GPa]	ν
FFM01	101061	71 ± 2[1]	0.30 ± 0.03
FFM02	101051	75 ±1	0.29 ± 0.005
FFM02	101058	77	0.29
FFM06	101057	80 ± 1	0.29 ± 0.02
DZ[2]	101057	71 ± 1	0.25 ± 0.01

[1]Note that the uncertainty is defined as "uncertainty of the mean", quantified for a 95% confidence interval.
[2] Deformation zone.

During site characterisation stage 2.3, rock samples containing sealed fractures from fracture domain FFM06 were also tested, proving that such fractures have no influence on the mechanical properties of the samples, which therefore present strength characteristics similar to those of intact rock samples.

The mechanical properties listed in

Table 2 and Table 3 were employed as initial values in the setup of the numerical model and underwent calibration procedures to obtain stress gradients consistent with the Martin (2007) model.

3.2.2 Mechanical properties of fractures

During site characterisation stage 2.2, samples containing fractures (both open and sealed) were collected within the target volume (RFM029 and RFM045), as well as in adjacent rock domains (RFM012, RFM034 and RFM044). The values of normal and shear stiffness that have been experimentally derived are listed in Table 4 as KN and KS, respectively.

Table 4. Mechanical properties of fractures from Site characterisation stage 2.2 for fracture domains FFM01 to FFM05 within the target volume for the construction of the repository (and in adjacent areas). After Glamheden et al. (2007b).

Fracture domain	KN [GPa/m]	KS [GPa/m] (@0.5 MPa)	KS [GPa/m] (@5.0 MPa)	KS [GPa/m] (@20 MPa)
FFM01	656 ± 396	10 ± 6	26 ± 9	34 ± 10
FFM02	248 ± 165	8 ± 4	26 ± 4	33 ± 8
FFM03	293 ± 193	8 ± 4	31 ± 7	35 ± 10
FFM04	1385 ± 283	8 ± 6	16 ± 5	23 ± 5
FFM05	599 ± 57	6 ± 3	20 ± 7	25 ± 2
DZ[1]	729 ± 662	12 ± 10	26 ± 9	31 ± 8

[1] Deformation zone.

Further mechanical properties were determined for the fractured samples collected during this stage of the site characterisation (e.g. dilatancy angle from direct shear tests, cohesion and friction, both peak and residual, from tilt tests), but were not necessary input data for the numerical modelling carried out in this study.

3.2.3 Rock mass mechanical properties

In site characterisation stage 2.2, two different approaches were employed to derive mechanical properties of the rock mass (fracture domains and deformation zones). The results of these two different studies (one empirical and one theoretical, i.e. based on numerical simulations) were harmonised to obtain a complete description of the quality of the rock mass (Glamheden et al. 2007b). It should be noted that the two approaches are based on substantially different techniques, resulting in the difficulty to reconciliate some key parameters at the base of the calculations. Some examples include:

- The scale over which the two evaluations are carried out, which varies between 5 m borehole sections (empirical approach) and 20 m x 20 m x 20 m (theoretical approach)
- The effect of confining pressure on some of the derived properties (e.g. not considered for Young's Modulus and Poisson's Ratio in the empirical methods).

A selection of the resulting (harmonised) rock mechanics properties in the target area (outside deformation zones) are presented in Table 5.

Table 5. Rock mass mechanical properties for areas outside of deformation zones from site characterisation stage 2.2. The values derive from the harmonisation of the results of empirical and theoretical calculations. After Glamheden et al. (2007b).

Fracture domain	E [GPa]	ν
FFM01	70 ± 8[1]	0.24 ± 0.03
(min-max)	39-79	0.12-0.33
FFM06	69 ± 12	0.27 ± 0.04
(min-max)	40-81	0.12-0.37

[1]Note that the uncertainty is defined as "uncertainty of the mean", quantified for a 95% confidence interval.

Within deformation zones, the harmonisation could not be carried out because the two approaches differ in a fundamental aspect of the calculations: while in the empirical approach the mechanical properties are derived assuming an isotropic body, the theoretical approach evaluates the same properties in an anisotropic fashion (parallel and perpendicular to the directions of the principal stresses).

In site characterisation stage 2.3, the empirical approach was employed again to characterise the rock mass specifically within the Singö and Forsmark deformation zones (Glamheden et al., 2008). The Singö deformation zone presents a high variability of the rock mass quality, probably reflecting a substantial heterogeneity within the deformation zone. The same variability was not observed within the Forsmark deformation zone, which also does not appear to be of substantially lower quality than the surrounding rock mass.

The results of the empirical evaluation of mechanical properties for the Singö and Forsmark deformation zones is presented in Table 6.

Table 6. Mechanical properties for the Singö and Forsmark deformation zones estimated by means of the empirical approach in site characterisation stage 2.3. After Glamheden et al. (2008).

Deformation zone	E [GPa]	ν
Singö	37.9 ± 9.4[1]	0.15 ± 0.04
(min-max)	21.2-78.5	0.08-0.32
Forsmark	38.3 ± 6.7	0.12 ± 0.03
(min-max)	23.9-52.3	0.07-0.18

[1]Note that the uncertainty is defined as "uncertainty of the mean", quantified for a 95% confidence interval.

4 WP3 – Numerical model

This Chapter illustrates the boundary conditions applied on the subsurface geological model in COMSOL Multiphysics, as well as the chosen material properties.

4.1 Boundary conditions

The following section describes the boundary conditions applied to the model. These have been parameterised to investigate the effect of different conditions on the stress field in the centre of the model.

4.1.1 Displacement boundaries

The vertical boundaries contain a parameterised, prescribed displacement pushing the outer boundaries inward and hence creating a compressive stress field within the modelling domain.

4.1.2 Roller boundaries

While the upper boundary is a free surface, the bottom boundary is a roller boundary allowing only boundary tangential displacements and is represented by

$$n \cdot u = 0$$

where u is the displacement vector and n is the boundary normal vector. The roller and displacement boundaries constrain the model.

4.1.3 Fracture zones

The fracture zones have been modelled as thin elastic layers with anisotropic stiffnesses. The fracture zones decouple the displacement fields on both sides and are then connected by elastic forces with equal size but opposite directions f_s, proportional to the relative displacements and velocities given by

$$f_{su} = -f_{sd} = K(u_u - u_d - u_0)$$

where K is the anisotropic spring constant per unit area and the subscripts u and d denote the "upside" and "downside" of the interior boundary, respectively. This allows displacements in both a tangential and a normal direction.

4.1.4 Vertical stress

The vertical stress is derived from the density of the rock by

$$S_V = \rho g z$$

where ρ is the rock density equal to 2.750 kg/m^3, g is the gravitational acceleration, and z is depth.

4.1.5 Pore Pressure

Similarly, the pore pressure is prescribed to the model by

$$P_o = \rho_f g z$$

where ρ_f is the fluid density of 1'020 kg/m^3 resulting in a pore pressure gradient of 10 MPa/km.

4.2 Implementation of solid mechanics in COMSOL Multiphysics

COMSOL Multiphysics uses the theory of linear elasticity to solve for the displacement and stress field within the modelling domain. Based on the conditions of equilibrium, in which all forces on the elastic body sum to zero, the equilibrium equation is:

$$0 = \nabla * S$$

S is the Cauchy stress tensor. Effective stresses are related to elastic strains via the following relationship, Hooke's law, also considering different external stress fields S_{ad} that can be super-positioned:

$$S = S_{ad} + \boldsymbol{C} : \epsilon$$

Here, S_{ad} is the pore pressure. The strain-displacement relationship is described by:

$$\epsilon = \frac{1}{2}\left[(\nabla u)^T + \nabla u\right]$$

ϵ is the strain tensor and $\boldsymbol{C}$ is the fourth order stiffness tensor. Deformation of the solid skeleton is described in terms of elastic response, considering the Young's modulus E, the Poisson's ratio ν, and the shear modulus G:

$$\boldsymbol{C} = \boldsymbol{C}(E,\nu,G)$$

The assumption of a linear elastic material behaviour is conservative as the stresses in the rock are not reduced due to an inelastic material behaviour.

4.3 Range of material properties

Stiffness of fracture zones are difficult to measure for smaller fractures; moreover, measured stiffness values of the same rock type under similar loading conditions can show a large variation of stiffness values due to complex interacting factors such as. fracture surface geometry, asperity deformability, fracture interlocking and testing conditions (Zangerl et al., 2008). However, Glamheden et al. (2007a) investigated the Singö fracture zone in detail and derived, for a range of 5 MPa to 20 MPa normal stresses, a normal and shear stiffness of 200 MPa/m and 10 MPa/m to 15 MPa/m, respectively. This contrasts with fracture stiffnesses of 656 GPa/m and 34 GPa/m in a normal and shear direction, respectively, given in Hökmark et al. (2010). These values provide a range of expected stiffnesses for the modelling campaign.

5 WP4 – Stress inversion

The range of material properties stated above implies that more than a set of boundary conditions and rock mass parameters might exist which yields the proposed in-situ stress field. The aim of the stress inversion is to find one set of boundary conditions and material properties that reproduce the overall proposed stress field. Once the proposed stress field is calibrated, the influence of the fracture zones on the large scatter in the measured stresses can be analysed. Therefore, the model parameters have undergone substantial iterations to determine an initial stress field closest to the measured values within reasonable ranges of boundary conditions and material parameters. These iterations are described in chapter 5.1 and have been performed on the model without considering the fracture zones. The pre-calibrated model has been further tuned by running parametric sweeps across fracture zone stiffnesses to gain a better understanding of the large variance in the measured stresses. This tuning is described in Chapter 5.2.

5.1 Calibration of initial stress field

An extensive iterative process was chosen to derive an in-situ average stress field closest to the stress field of Martin (2007). Multiple variations of the inward directed displacement of the vertical boundaries, as well as the elastic properties of the rock mass (Young's modulus and Poisson's ratio) were carried out.

At an early stage of the modelling campaign, depth-dependent displacement magnitudes were tested, which did however not result in increasing stress gradients throughout the entire model domain, as these heterogeneous strains would homogenize after a short lateral distance (Saint-Venant's principle). Hence, inward directed depth-constant displacement magnitudes between 0 m and 20 m were tested on all four vertical boundaries. The best fit was obtained for displacements of 9 m in SH direction (NW-SE) and 2.25 m in Sh direction (NE-SW). These displacement magnitudes proved to be necessary to stay within the range of expectable rock mass parameters. It was found that compression solely in SH-direction could not explain the stress field proposed by Martin (2007), as Sh-magnitudes would be too small.

Young's modulus and Poisson's ratio were tested in the ranges given in Chapter 3. Key findings of this iterative approach are:

- an increase in depth-constant Poisson's ratio is increasing the magnitude of the horizontal stresses but is not able to produce the expected horizontal stress gradient with depth,
- constant Young's moduli do not yield high enough stress gradients,
- Young's moduli linearly increasing with depth are necessary to reach the expected stress gradients,
- an orthotropic distribution of Young's moduli is needed to obtain correct SH-Sh-ratios,
- within the frame of our initial model conditions a depth-dependent, orthotropic material tensor is best suited to describe the stress field by Martin (2007). This is further discussed in Chapter 7.

In our calibrated model the Young's modulus in Sh direction (NE-SW) is increasing slightly from 32 GPa to 35 GPa from 150 m to 400 m and increases monotonically to 46.7 GPa at 600 m depth. Similarly, the Young's modulus in SH direction (NW-SE) is increasing from 30 GPa to 50 GPa from 150 m to 400 m and increases monotonically to 53 GPa at 600 m depth (Figure 6). For depths larger than 600 m, which is for depth larger than the stress model of Martin (2007), the Young's modulus increased linearly to 75 GPa at the bottom of the model at 2,200 m (Figure 7). This corresponds to the average Young's modulus from modelling stage 3

(Glamheden et al., 2008). For all depths resulting stresses are within the error margin of Martin (2007).

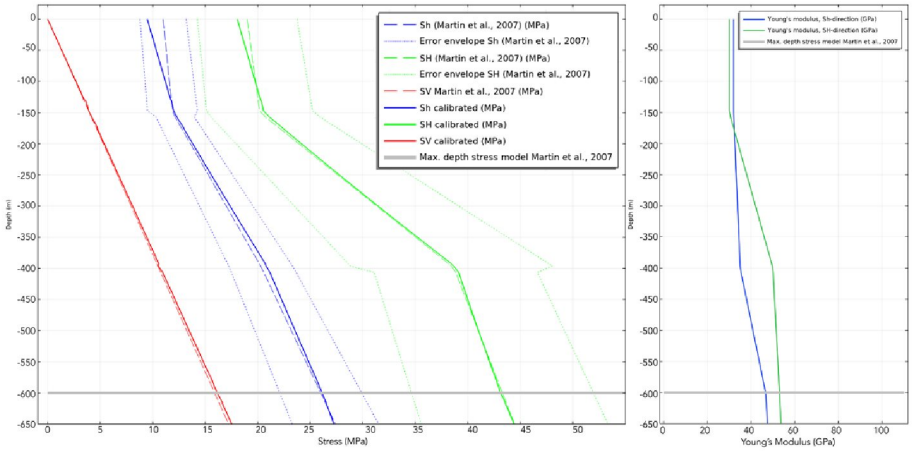

Figure 6 Calibrated stress field and Young's modulus for the depth interval covered by Martin (2007). Left: modelled (solid lines) versus stress field derived by Martin (2007; dashed lines) including error envelopes (dotted lines). Right: Young's modulus in Sh-direction (blue) and SH-direction (green). Grey horizontal line indicates maximum depth of stress model by Martin (2007).

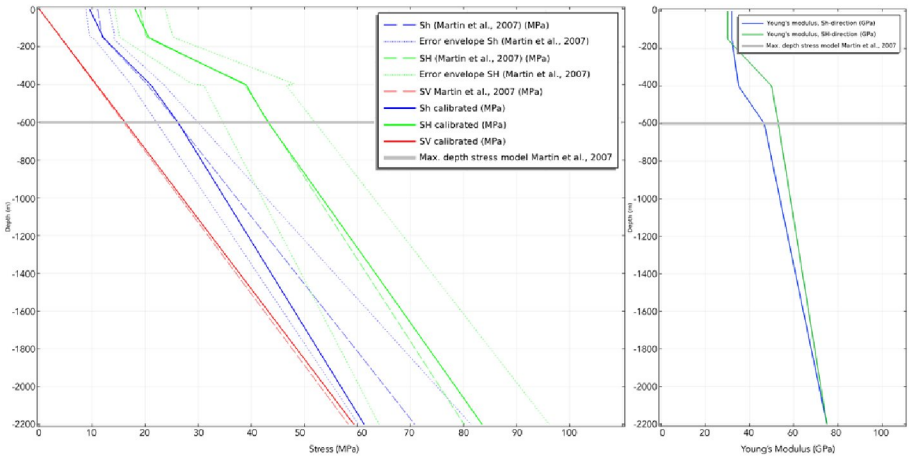

Figure 7 Calibrated stress field and Young's modulus for the entire depth of the model. Left: modelled (solid lines) versus stress field derived by Martin (2007; dashed lines) including error envelopes (dotted lines). Right: Young's modulus in Sh-direction (blue) and SH-direction (green). Grey horizontal line indicates maximum depth of stress model by Martin (2007).

5.2 Parametric sweeps – fracture zone parameters

While the model developed with the aforementioned characteristics fits nicely with the overall stress curves proposed by Martin (2007), local measurements derived from the overcoring and/or hydraulic testing campaigns still deviate (at times significantly) from the modelled stresses.

In order to investigate these differences in more detail, and to understand the effect of specific fracture zone parameters on the variability of stress measurements, two parametric sweep studies were run on sub-horizontal fracture zones intersected by boreholes used for stress field estimation. In particular, normal (k_n) and shear (k_s) stiffnesses were varied for 3 different fracture zones (see Figure 8 and Figure 9) along a range spanning from 0.1 GPa/m to 20 GPa/m (normal stiffness) and from 0.01 GPa/m to 2 GPa/m (shear stiffness), while the normal-to-shear stiffness was maintained at 10:1. Vertical to sub-vertical fault zones have not been parameterised due to the larger distance to the stress measurements and their expected reduced influence on the stress field at these positions.

For stiffnesses higher than the combination k_n=20 GPa/m and k_s=2 GPa/m no effect was observed on the modelling results (see e.g. Figure A5 and Figure B3). Higher values are hence not expected to have a significant or realistic influence on the modelling results.

The ranges of values employed in the parametric sweeps do not exclude the possibility for the fracture zones to be substantially weakened by clay alteration in the damage zone core, while also considering values (10-20 GPa/m) more typical of joints in granite or basalt with little to no damage zone (e.g. Kulhawy 1975, Bandis et al., 1983).

The first parametric study focused on a sub-horizontal fracture zone (Figure 8) penetrated by the DBT-1 borehole at –445 m, which was used for overcoring tests. The second parametric study varied the stiffnesses of two fracture zones (Figure 9) which are both cross-cut by the KFM02A borehole at -530 m and -600 m, along which hydraulic fracturing tests were conducted.

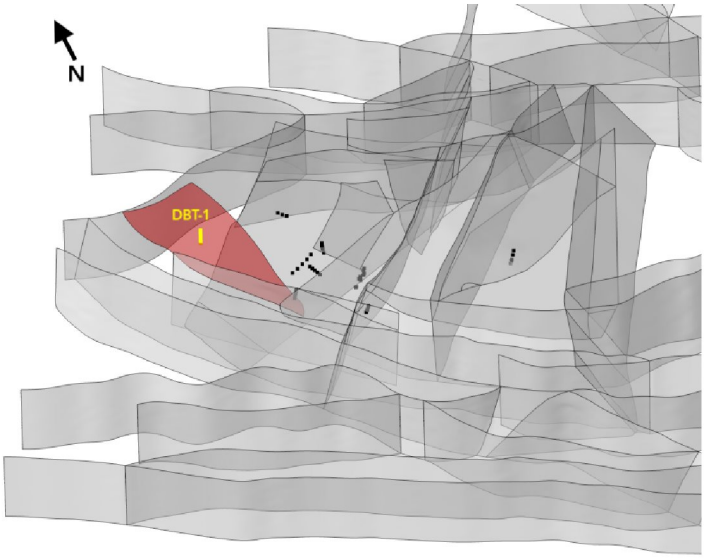

Figure 8 In red, the fracture zone that is intersected by borehole DBT-1 at -445 m, along which overcoring tests were carried out to estimate the magnitude and orientation of the stress field in the area (in yellow, the data points representing overcoring measurements; the data points of the further overcoring tests carried out in other boreholes in the area are displayed in the figure as black dots). The stiffnesses of this fracture zone were varied in the first of two parametric sweeps, the results of which are presented in section 6.3.

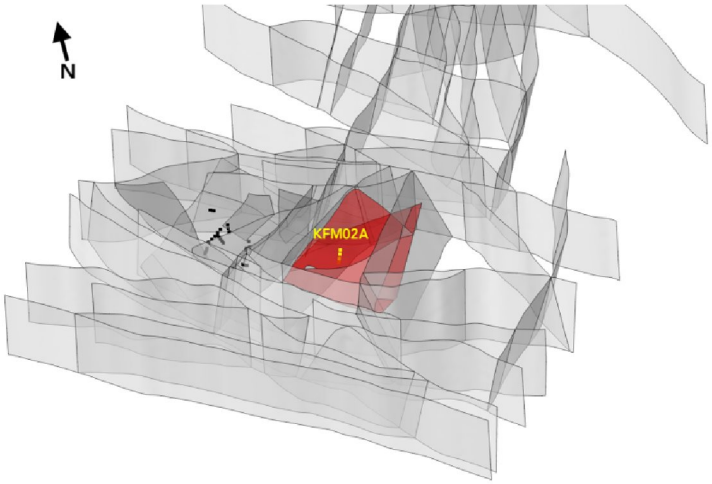

Figure 9 In red, the fracture zones that are intersected by borehole KFM02A at -530 and -600 m, along which hydraulic fracturing tests were carried out to estimate the magnitude and orientation of the stress field in the area (in yellow, the data points representing hydraulic test measurements; the data points of the further hydraulic tests carried out in other boreholes in the area are displayed in the figure as black dots). The stiffnesses of these fracture zones were varied in the second of two parametric sweeps, the results of which are presented in section 6.4.

5.3 Parametric study 1 – comparison with overcoring measurements

The first parametric sweep was run for the model assuming variations in stiffness (both normal and shear) only for the fracture zone ZFMB8 (more details cf. Stephens & Simeonov 2015), which is intersected by the DBT-1 borehole (see Figure 8). All other fracture zones (both vertical and sub-horizontal) are treated as stiff surfaces along which no normal or shear movement is permitted.

In Table 7, the results of the overcoring tests carried out in the DBT-1 borehole are shown in terms of magnitude, trend and plunge of the three principal stresses.

The intersection with the fracture zone being tested in this parametric study occurs at a depth of approx. -445 m.

Table 7 Results of the overcoring tests carried out in the DBT-1 borehole.

Hole length	Depth	Magnitude [MPa]			Trend [°]			Plunge [°]		
[m]	[m]	S1	S2	S3	S1	S2	S3	S1	S2	S3
13.87	13.87	14.0	11.2	-3.8	99	9	196	1	8	82
31.36	31.36	35.5	18.4	6.0	87	356	249	12	4	78
31.96	31.96	30.0	16.8	-3.2	58	326	185	10	12	75
50.37	50.37	12.6	4.5	1.1	9	103	256	9	19	69
71.40	71.40	14.1	7.3	-11.1	308	218	57	3	9	81
90.00	90.00	18.8	6.7	-3.1	341	250	114	5	6	82
90.62	90.62	29.5	21.0	-3.8	268	178	18	3	7	82
133.61	133.61	15.1	13.8	2.5	155	246	35	6	10	79
134.18	134.18	15.4	11.2	6.6	305	41	161	21	14	65
134.74	134.74	19.0	15.2	4.2	324	70	175	44	16	42
136.41	136.41	18.5	12.2	6.9	285	19	126	26	9	63
165.54	165.54	13.3	12.0	4.5	49	318	208	6	2	84
166.80	166.80	24.2	16.6	4.4	275	9	162	10	21	67
194.77	194.77	22.2	19.0	6.7	275	185	15	2	11	79
195.39	195.39	19.2	11.3	-5.4	283	13	111	9	1	81
218.90	218.90	20.6	18.1	5.4	329	238	144	26	2	64
219.63	219.63	25.8	17.4	4.4	181	85	336	27	10	61
246.94	246.94	18.4	11.1	9.0	45	135	311	1	12	78
275.65	275.65	40.5	21.4	8.4	323	55	222	4	18	71
276.31	276.31	38.0	20.3	9.9	270	0	102	8	2	82
299.71	299.71	21.8	13.9	9.3	311	43	180	11	12	73
300.34	300.34	32.0	10.6	1.5	332	241	149	29	2	61
374.63	374.63	42.5	29.7	5.8	148	57	275	6	7	81
377.37	377.37	42.8	28.0	3.8	162	71	273	7	17	72
378.16	378.16	47.2	22.1	3.3	122	32	275	7	3	83
422.59	422.59	63.1	43.2	12.7	128	38	233	3	10	80
460.48	460.48	60.4	33.1	21.2	139	229	319	10	0	81
485.72	485.72	67.0	48.7	29.0	302	36	190	9	22	66
499.87	499.87	56.9	28.8	16.1	159	249	354	4	1	85
501.76	501.76	54.1	36.6	13.7	154	63	266	4	11	78

The combination of stiffness values that are tested in our parametric study are listed in Table 8, following the convention for which k_n is typically one order of magnitude larger than k_s. Only one combination was tested, in which the normal-to-shear stiffness ratio was three instead of one order of magnitude. This was done to test whether a potentially unusual (but still possible) combination of stiffnesses could lead to better results in the comparison of the modelled magnitudes with the measured ones.

Table 8 The combinations of normal and shear stiffness values that were tested in parametric study 1.

kn [GPa/m]	ks [GPa/m]
0.1	0.01
1	0.1
10	1
20	2
10	0.01

In the following (and in Appendix A), pairs of figures referring to specific combinations of k_n and k_s values are presented together to discuss the results of the parametric study. In the first item of the pair, the stress curves resulting from the model are plotted against depth along a profile containing the vertical trace of the DBT-1 borehole. In the same figure, reference stress curves and their error envelopes are also shown from Martin (2007), as well as the data points representing the magnitudes of the three principal stresses measured in the DBT-1 borehole. The second figure of the pair contains a graph where the absolute magnitude difference between measured and modelled stress is plotted against depth per data point. The formula used to calculate the difference is the following:

$$\Delta Sx = |Sx_{measured} - Sx_{modelled}| \qquad [1]$$

where Sx can be any of the three principal stresses, S1, S2 or S3.

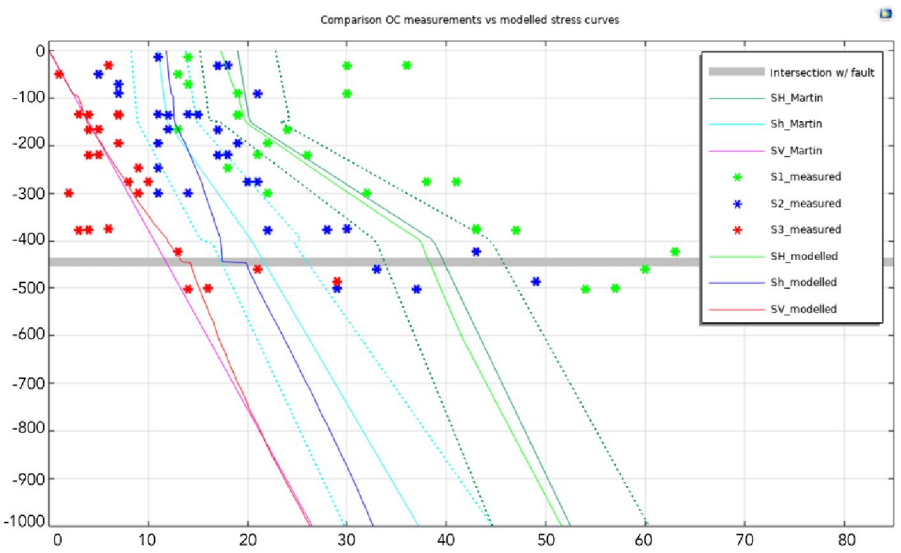

Figure 10 Comparison of the overcoring measurements collected in the DBT-1 borehole (shown as asterisks) and the stress curves modelled with k_n=0.1 GPa/m and k_s=0.01 GPa/m. The stress curves proposed by Martin (2007) are also shown (including the uncertainty envelopes, as stippled lines).

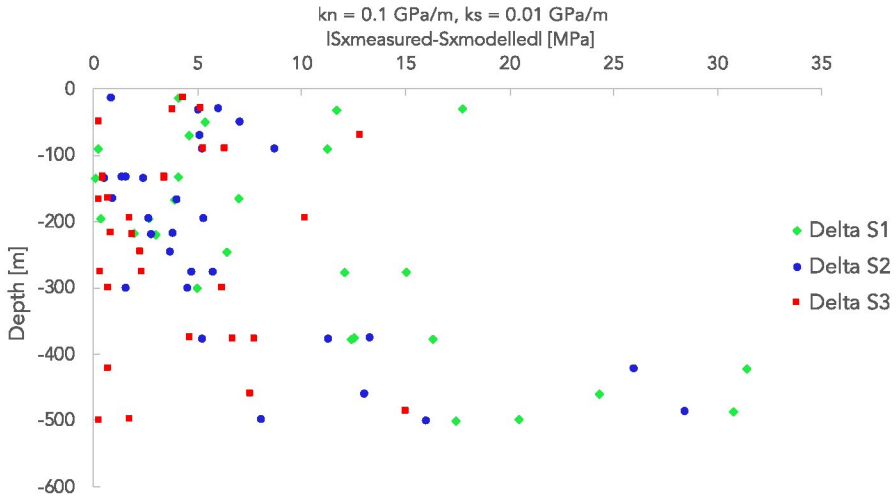

Figure 11 Difference between measured and modelled stress magnitudes for k_n=0.1 GPa/m and k_s=0.01 GPa/m plotted against depth. All three principal stresses are represented in the graph, in different colours.

In Figure 10 and Figure 11, the results of the first combination of stiffnesses can be seen. The modelled stress curves appear to be indeed affected by the presence of a fracture zone with low stiffness values (k_n=0.1 GPa/m and k_s=0.01 GPa/m; see the small kink in the curves corresponding to the grey line, particularly evident for Sh and SV; Figure 10). A substantial divergence between measured and modelled stresses is, however, already observed at shallower depths (ca. -370 m depth, see also Figure 11) and is continuously increasing down to the maximum depth of measurement (-502 m). Still in Figure 10 it is evident how these measured magnitudes (below ca. -370 m) differ considerably from the stress curves proposed by Martin (2007), as well as from our modelling results.

In Figure 12 and Figure 13, the results from the combination of values k_n=10 GPa/m and k_s=0.01 GPa/m are plotted. Note how the kink corresponding to the intersection with the fracture zone is still visible in all stress curves, albeit less pronounced than in the combination with a lower normal stiffness (Figure 12). As a result, the values of ΔSx are not improved with respect to the first combination of stiffness values (Figure 13).

The following combinations of normal and shear stiffness (Figure A1 to Figure A6) show only minor variations in the modelling results, with the effect of the intersecting fracture zone progressively disappearing from all the three stress curves with increasing stiffness. Therefore, no substantial improvement of the absolute $\Delta S1$, $\Delta S2$ and $\Delta S3$ could be achieved by varying the parameters of the intersected fracture zone.

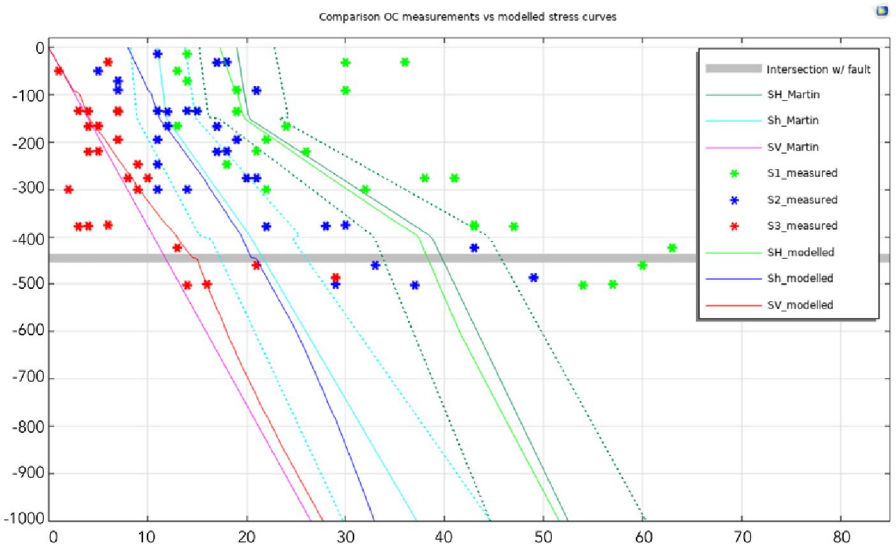

Figure 12 Comparison of the overcoring measurements collected in the DBT-1 borehole (shown as asterisks) and the stress curves modelled with k_n=10 GPa/m and k_s=0.01 GPa/m. The stress curves proposed by Martin (2007) are also shown (including the uncertainty envelopes, as stippled lines).

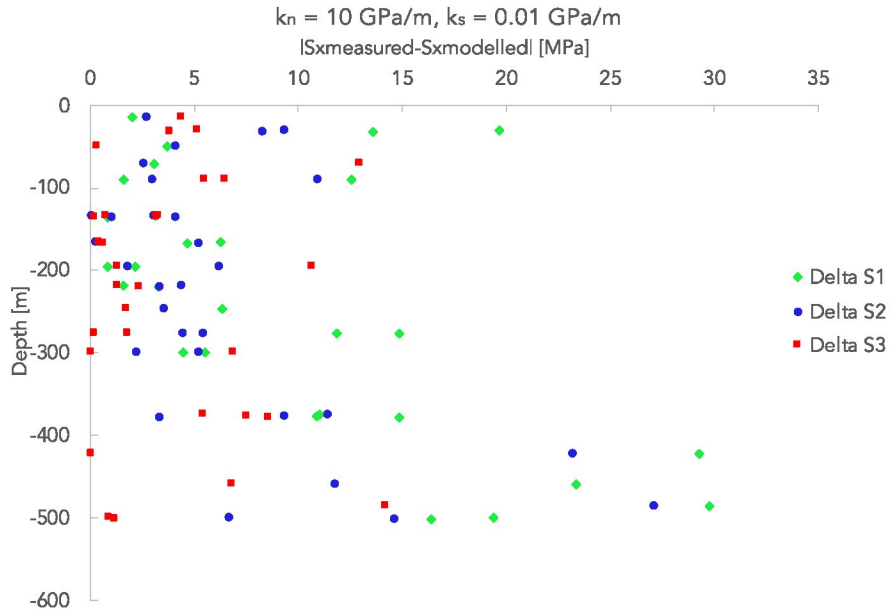

Figure 13 Difference between measured and modelled stress magnitudes for k_n=10 GPa/m and k_s=0.01 GPa/m plotted against depth. All three principal stresses are represented in the graph, in different colours.

In an effort to more directly evaluate the accuracy of the results of the parametric sweep with respect to the measured values, Table 9, Table 10 and Table 11 compare the mean, median and standard deviation of the ΔSx value (in MPa, see equation [1]) calculated for each combination of normal and shear stiffness. A minor improvement (slight decrease in the mean and standard deviation values) can be observed for $\Delta S1$ and $\Delta S2$ with increasing stiffnesses, while the effect is less pronounced (or even inverted) for $\Delta S3$. Note that the combination k_n=10 GPa/m and k_s=0.01 GPa/m (i.e. the only one that deviates from the condition k_n=10*k_s) does not

produce substantially worse or better results than the other combinations tested for any of the three principal stresses.

Table 9 ΔS1 mean, median and standard deviation values (in MPa) for different combinations of k_n and k_s and for a reference model without the weak fracture zone.

	|S1measured - S1modelled|					
	0.1 – 0.01	1 – 0.1	10 - 1	20 - 2	10 – 0.01	Reference
Mean	9.73	8.80	8.61	8.60	9.36	8.58
Median	5.91	7.61	7.30	7.24	5.92	7.18
St. dev.	8.61	7.53	7.25	7.23	8.31	7.21

Table 10 ΔS2 mean, median and standard deviation values (in MPa) for different combinations of k_n and k_s and for a reference model without the weak fracture zone.

	|S2measured – S2modelled|					
	0.1 – 0.01	1 – 0.1	10 - 1	20 - 2	10 – 0.01	Reference
Mean	6.86	6.41	6.33	6.33	6.64	6.32
Median	5.10	4.43	4.36	4.37	4.42	4.37
Std. dev.	6.64	5.97	5.89	5.88	6.10	5.88

Table 11 ΔS3 mean, median and standard deviation values (in MPa) for different combinations of k_n and k_s and for a reference model without the weak fracture zone.

	|S3measured – S3modelled|					
	0.1 – 0.01	1 – 0.1	10 - 1	20 - 2	10 – 0.01	Reference
Mean	3.96	3.99	4.04	4.04	3.95	4.05
Median	2.92	2.87	2.97	2.98	2.80	2.99
Std. dev.	3.78	3.83	3.82	3.83	3.84	3.83

However, what mostly transpires from the results of the parametric sweep is the substantial independence of the modelled stress magnitudes from the mechanical behaviour of the sub-horizontal fracture zones whose parameters were varied in this study. Moreover, the standard deviation is rather large for all datasets, indicating a substantial dispersion of the ΔSx values. A reason for this can be found in the original scatter of the measured magnitude dataset.

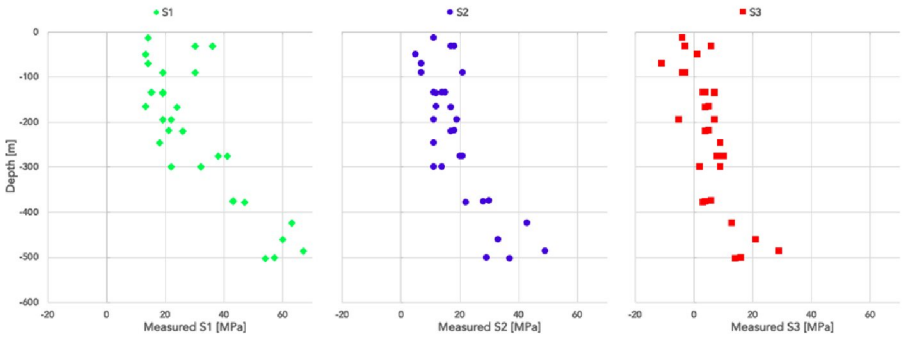

Figure 14 Data scatter of the measured S1, S2 and S3 magnitudes, plotted versus depth.

In Figure 14, the measured data points for all three principal stresses are plotted against depth; the large variability of the magnitude data is evident, particularly for

S1 (with variations of up to ca. 25 MPa, e.g. within the shallowest 50 m) and S2 (up to ca. 20 MPa difference between values measured within less than 20 m in depth).

5.4 Parametric study 2 – comparison with hydraulic fracturing measurements

The second parametric sweep carried out on the model consisted in the variation of both normal and shear stiffness for two intersecting sub-horizontal fracture zones that are cross-cut by the KFM02A borehole at depths of ca. -530 m and -600 m, respectively. The combinations of normal and shear stiffness values that were used in the study are the ones listed in Table 8. Magnitude, trend and plunge values of the three principal stresses as measured in the KFM02A borehole are presented in Table 12.

As for the results presented in the first parametric study, two figures are presented per combination of stiffness values. In the first graph, the modelled curves are plotted together with the reference Martin (2007) stress curves (and their uncertainty envelopes); the measured values of magnitude for S1, S2 and S3 are also shown in the graph, as asterisks.

In the second figure of the pair the absolute difference between modelled and measured stress magnitudes (as per equation [1]) is plotted versus depth.

Table 12 Results of the hydraulic tests carried out in the KFM02A borehole.

Hole length [m]	Depth [m]	Magnitude [MPa]			Trend [°]			Plunge [°]		
		S1	S2	S3	S1	S2	S3	S1	S2	S3
220.70	220.09	11.8	7.1	5.8	110	200	0	0	0	90
223.50	222.88	10.7	6.8	5.9	125	215	0	0	0	90
376.00	374.78	15.9	8.7	9.9	24	114	0	0	0	90
551.00	549.53	32.9	16.4	14.6	128	218	0	0	0	90
603.00	600.58	37.5	18.3	15.9	137	227	0	0	0	90
701.50	698.30	44.5	21.6	18.5	142	232	0	0	0	90
704.30	701.08	47.5	22.6	18.6	136	226	0	0	0	90

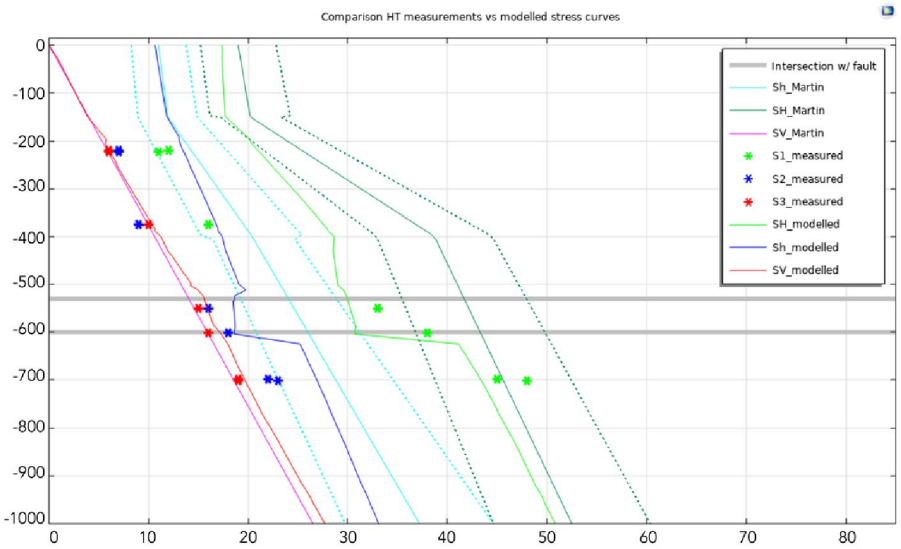

Figure 15 Comparison of the hydraulic test measurements collected in the KFM02A borehole (shown as asterisks) and the stress curves modelled with k_n=0.1 GPa/m and k_s=0.01 GPa/m. The stress curves proposed by Martin (2007) are also shown (including the uncertainty envelopes, as stippled lines).

In Figure 15, the modelled curves resulting from the combination of values k_n=0.1 GPa/m and k_s=0.01 GPa/m (adopted for both fracture zones cross-cut by the KFM02A borehole) are shown. Beside deviating substantially from the reference Martin (2007) curves (also considering the uncertainty envelopes), the modelling results do not achieve a good fit with the measured data (with the exception of the S1 values measured below ca. -530 m, which plot somewhat near the modelled S1 curve). This divergence is quantified in Figure 16, where the absolute difference between modelled and measured magnitude values (according to equation [1]) for all three principal stresses are plotted against depth.

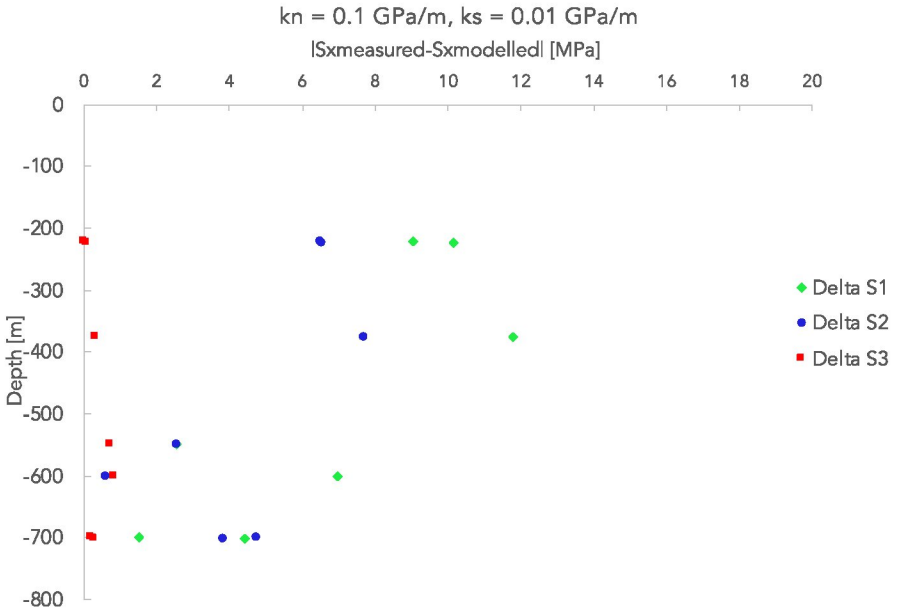

Figure 16 Difference between measured and modelled stress magnitudes for k_n=0.1 GPa/m and k_s=0.01 GPa/m plotted against depth. All three principal stresses are represented in the graph, in different colours.

The next combination of stiffnesses tested in our study (k_n=1 GPa/m and k_s=0.1 GPa/m) brings the modelled stresses more in line with the reference from Martin (2007), i.e. within the uncertainty envelopes, but does not improve the fit with the measured values (see Figure 17 and Figure 18).

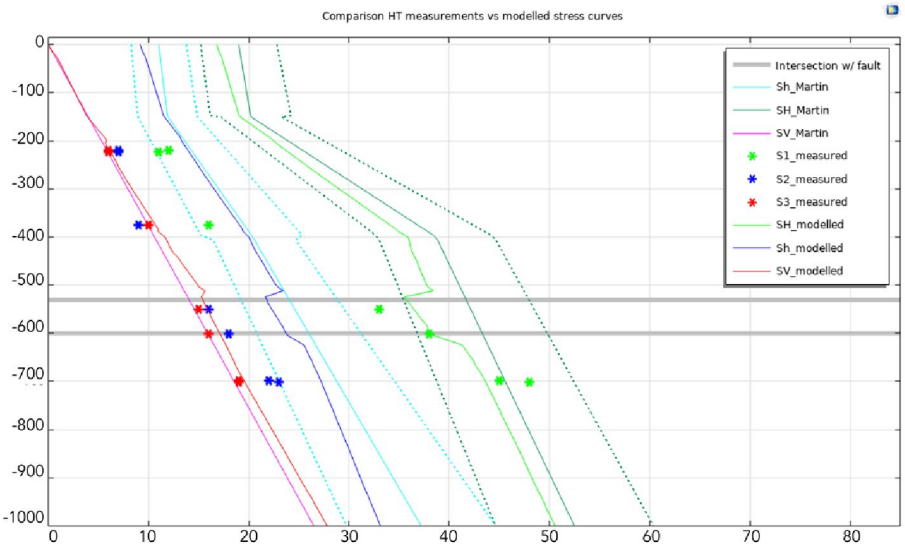

Figure 17 Comparison of the hydraulic test measurements collected in the KFM02A borehole (shown as asterisks) and the stress curves modelled with k_n=1 GPa/m and k_s=0.1 GPa/m. The stress curves proposed by Martin (2007) are also shown (including the uncertainty envelopes, as stippled lines).

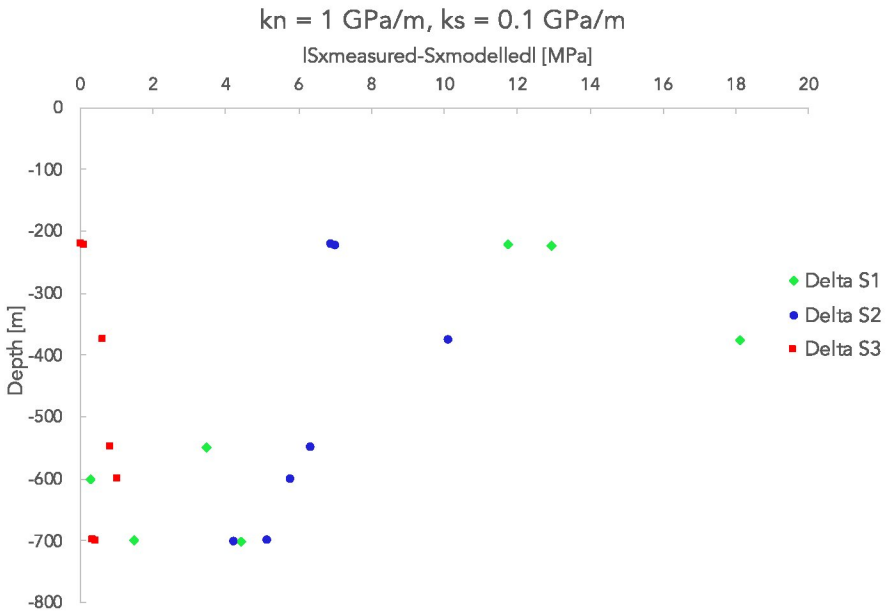

Figure 18 Difference between measured and modelled stress magnitudes for k_n=1 GPa/m and k_s=0.1 GPa/m plotted against depth. All three principal stresses are represented in the graph, in different colours.

The model with k_n=10 GPa/m and k_s=0.01 GPa/m produces a substantial change in the general trends of the modelled stress curves (Figure 19); a marked increase in magnitude of all three stresses is observed in correspondence with the first of the two intersecting fracture zones, while the presence of the second appears to be mostly affecting S1. This is accompanied by generally low magnitudes for S1 and S2 at shallower depths. This scenario represents an improvement in the comparison with the measured values with respect to the k_n=1 GPa/m and k_s=0.1 GPa/m combination, but does not differ quantitatively from the study with the same shear stiffness and k_n=1 GPa/m (compare Figure 20 with Figure 18 and Figure 16).

The rest of the combinations tested (which can be found in Appendix B; see Figure B1 to Figure B4) produce even worse fits with the measured magnitudes.

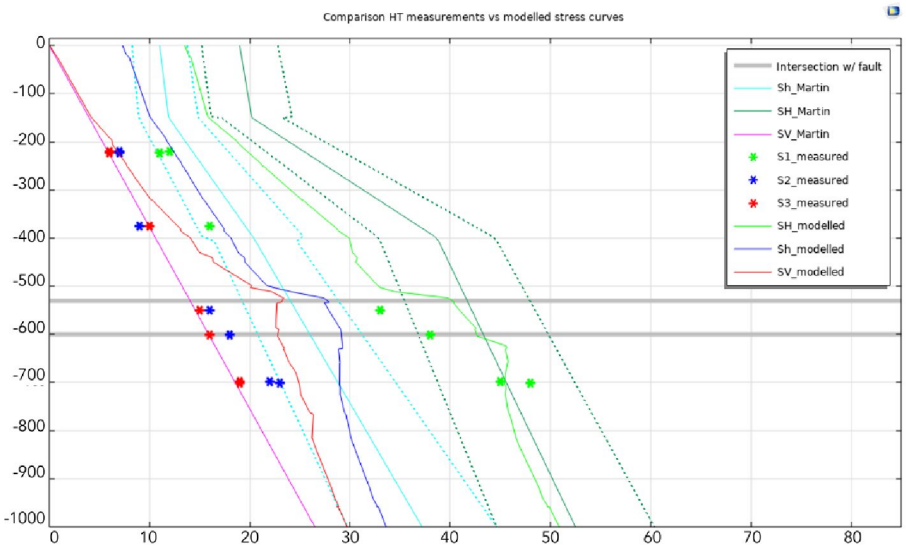

Figure 19 Comparison of the hydraulic test measurements collected in the KFM02A borehole (shown as asterisks) and the stress curves modelled with k_n=10 GPa/m and k_s=0.01 GPa/m. The stress curves proposed by Martin (2007) are also shown (including the uncertainty envelopes, as stippled lines).

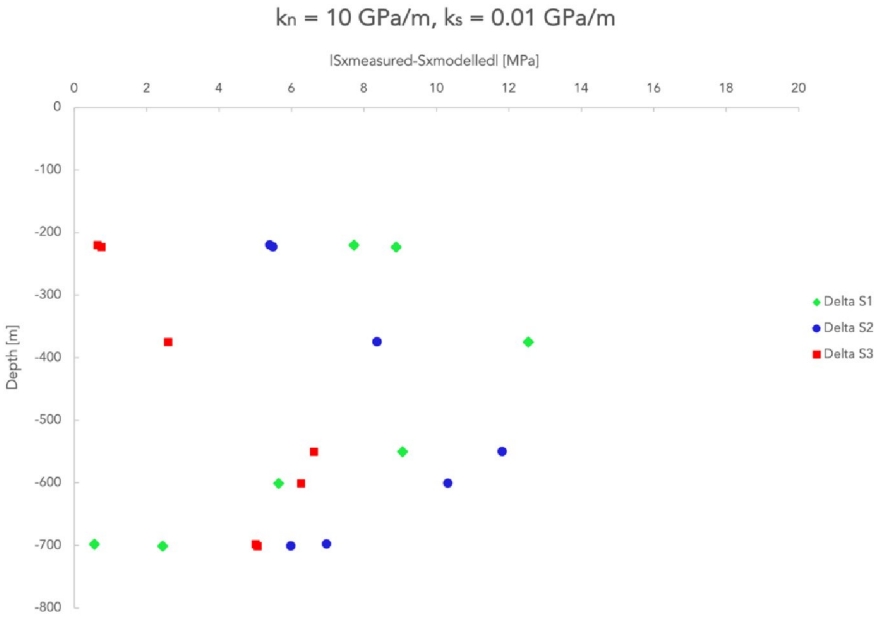

Figure 20 Difference between measured and modelled stress magnitudes for k_n=10 GPa/m and k_s=0.01 GPa/m plotted against depth. All three principal stresses are represented in the graph, in different colours.

As for the first parametric sweep, three tables were compiled to facilitate the quantification and comparison of the results from the different stiffness scenarios. In Table 13, Table 14 and Table 15 the arithmetic mean, median and standard deviation values of the different ΔSx datasets are compared; a column is added where the three ΔSx are calculated also for a reference model in which the two fracture zones are stiff surfaces allowing for no slip.

Table 13 ΔS1 mean, median and standard deviation values for different combinations of k_n and k_s and for a reference model without the weak fracture zones.

	|S1measured - S1modelled|					
	0.1 – 0.01	1 – 0.1	10 - 1	20 - 2	10 – 0.01	Reference
Mean	6.63	7.50	8.55	8.63	6.69	8.71
Median	6.96	4.43	6.22	6.49	7.73	6.79
Std. dev.	3.64	6.25	5.94	5.92	3.83	5.89

Table 14 ΔS2 mean, median and standard deviation values for different combinations of k_n and k_s and for a reference model without the weak fracture zones.

	|S2measured – S2modelled|					
	0.1 – 0.01	1 – 0.1	10 - 1	20 - 2	10 – 0.01	Reference
Mean	4.63	6.50	6.85	6.88	7.77	6.91
Median	4.74	6.33	6.95	6.98	6.97	7.05
Std. dev.	2.33	1.73	1.80	1.81	2.33	1.82

Table 15 ΔS3 mean, median and standard deviation values for different combinations of k_n and k_s and for a reference model without the weak fracture zones.

	|S3measured – S3modelled|					
	0.1 – 0.01	1 – 0.1	10 - 1	20 - 2	10 – 0.01	Reference
Mean	0.36	0.49	0.15	0.12	3.85	0.11
Median	0.28	0.43	0.10	0.05	5.01	0.04
Std. dev.	0.29	0.33	0.15	0.13	2.32	0.11

The compilation of results presented in Table 13, Table 14 and Table 15 shows, here as well, that the mechanical behaviour of single fracture zones is not sufficient to obtain a good correspondence between the measured and the modelled values for stress magnitudes in the region of interest, regardless of the parameters tested (from very weak to stiff fracture zones).

In the case of the hydraulic tests carried out in the KFM02A borehole, moreover, the dataset of measured values can be questioned in both regarding the low number of data points (7) and the reliability of the measured magnitudes (with extremely low values at shallow depths, particularly for S2 and S1); this latter fact was also underlined by Martin (2007), which ultimately excluded the hydraulic measurements from his estimation of a stress model for the area.

6 WP5 – Stress validation

The work package has been proposed initially for fine tuning of the stress conditions after the parametric sweep. However, due to the small influence of the fault zone properties on the stress field, this work package has become obsolete.

7 Discussion- uncertainties and recommendations

The numerical model developed for the Forsmark lens is the result of an integrated study based on the elaboration of geomechanical concepts applied to a structurally complex rock mass. The input data for the model included the geometrical elements that characterise the region of interest at the km scale (i.e. the fault network), measurement data collected over various campaigns for the determination of the in-situ state of stress, experimentally derived values for the main geomechanical properties of the rock mass as well as the interpretations of said measured and derived parameters formulated at different stages of the site characterisation process.

The complexity of the structural elements and the high variability of many of the input parameters and data collected in the area generated uncertainties in the resulting numerical model. In what follows, we discuss the main sources of uncertainty in greater detail.

7.1 Uncertainties in the subsurface model

The subsurface model is based on geometric data provided by SKB. The accuracy of the data was not questioned, and uncertainties regarding the data (e.g. geometrical uncertainty of fracture zone localisation, strike and dip angles etc.) are neglected in this report. Some of the delivered fracture zones had to be simplified, and not all fracture zones were implemented in the final subsurface model. The regional scale fracture zones not implemented in the model are all situated outside the region of interest, i.e. outside the Forsmark lens. The decision not to implement all fracture zones was based on a generic internal feasibility study, showing that the effect of the fracture zones on the stress field are very small and spatially constrained. The final study further reinforced the decision, as it was shown that the effect of the fracture zones on the stresses inside the region of interest is negligible, indicating that the influence of the missing fracture zones (outside the region of interest) is also negligible. This is in line with the initial concept for the location of the repository within a tectonic lens, where the surrounding major fault zones should encapsulate the repository and leave the bedrock less affected by deformations.

For this study, only the fracture zones mapped on the regional scale were used and the local scale fracture zones were not considered. The intent was to first study the effect of the large structures before investing a large amount of time in the even more complex model creation for the local fracture zones. This has proven to be a sensible approach, as it was shown that the influence of the large fracture zones is negligible, indicating that the implementation of the local-scale fracture zones would lead to even smaller and thus irrelevant stress alterations.

Furthermore, the topography and seawater in the Forsmark region were not implemented in the subsurface model, as the implementation would have been very labour intensive, while the resulting stress changes would have been minimal and inside the error margin of the Martin (2007) stress field. Lastly, the subsurface model does not contain explicitly modelled rock domains to account for different rock mass parameters. Instead, implicit depth dependent changes of the material properties were applied. The implementation of geometrically complex rock domains partially intersecting and interacting with the fracture zones would have been extremely labour intensive; a generic internal feasibility study indicated that the difference between explicit and implicit material property changes in the region of interest is negligible.

The calibration of the model indicated that additionally to the compression in SH-direction (i.e. NW-SE) further compression in Sh-direction (i.e. NE-SW) is needed to match the stress field in the Forsmark region. This compression in Sh-direction is needed to obtain Sh stresses exceeding the vertical stress SV, as is the case in the reverse faulting regime expected for Forsmark. Without the compression in Sh-direction Sh would be a result of the vertical stress and the Poisson's ratio and could not exceed SV. The amount of compression applied in SH-direction (9 m) and in Sh-direction (2.25 m) are a direct result of the model calibration and are only applicable for the range of elastic parameters documented for the rock mass in Forsmark. Different rock mass parameters would necessitate different displacements. In addition to varying but depth-constant displacement magnitudes, depth-dependent displacement magnitudes were additionally tested at an early stage of the modelling campaign. Displacement magnitudes increasing with depth did however not result in increasing stress gradients throughout the entire model domain, as these heterogeneous strains would homogenize after a short lateral distance (Saint-Venant's principle).

7.2 Uncertainties in the material parameters

In Chapter 3.2, a brief summary of the input data available at the beginning of the project is presented.

The effort from SKB to fully characterise the target site from a multidisciplinary (geological) perspective has been considerable and has resulted in a large amount of data which often presents some variability.

According to the sampling and modelling campaigns conducted by SKB, the rock mass at Forsmark presents rather homogeneous rock quality characteristics (although evidences for a substantial heterogeneity of the mechanical properties within and around deformation zones are uncovered; e.g. the Singö deformation zone, cf. Glamheden et al., 2008). The main argument for this conclusion is the relatively little spread of experimentally estimated values of material properties for the intact rock samples. Some caution should however be exercised in the use of the values proposed by SKB, as a number of uncertainties could point to an underestimation of the rock mass inhomogeneity.

As discussed already in Glamheden et al., 2007b, the focus of the Complete Site Investigation campaigns has always been that of testing the proposed repository depth (i.e. -400 m to -500 m) within the two target fracture domains (i.e. FFM01 and FFM06). Consequently, the number of samples collected and tested outside this specific rock volume is comparatively small, which, among other ambiguities, results in some uncertainties in the extrapolation of the parameters at shallower as well as greater depths. Moreover, the necessity for SKB to keep the number of drilled wells to a minimum (in order to avoid the creation of possible fluid pathways into the future repository) further restricted the rock volume being tested. The sampling strategy could itself present some bias bound to affect the variability of the derived values: as mentioned above, inhomogeneities were introduced in the sampling of different fracture domains as well as rock types, and the selection of core sections for intact rock sampling was done purposedly avoiding fractured intervals or sections containing other kinds of imperfections. Moreover, indications of possible stress-induced microcracking affecting some of the tested core material are mentioned in Glamheden et al. (2007b), introducing a further element of variability in the derived values. Finally, some of the planned inter-laboratory comparisons to assess the variability of the experimental results between testing facilities could not be carried out (Glamheden et al., 2007b), so that related uncertainties cannot be ruled out.

While it is difficult to quantify the accumulated uncertainty in the material parameters, generated by all the mentioned uncertainties, it is reasonable to suggest that the overall heterogeneity of the rock volume could be at least partially underestimated. As mentioned, local (at times considerable) heterogeneities are recognised within and around deformation zones; given the complexity of the tectonometamorphic evolution of the area, as well as the relative lithological variations within the region of interest, further sources of uncertainty could have been overlooked and not properly sampled.

As a result, the model we propose is characterised by an orthotropic material behaviour for the rock volume, where the increase of the Young's modulus with depth is different in the directions parallel and perpendicular to the major principal stress. While the testing conducted on intact rock core samples does not support this hypothesis, the gradients for SH and Sh proposed by Martin (strongly converging with depth) cannot be reproduced for a completely isotropic body. We believe our choice is further justified by the mentioned sampling bias, which could have overlooked the effect of preferentially oriented sets of fractures and other structures on the overall material behaviour of the rock volume as a whole.

It should also be noted that our model, in accordance with Martin (2007), defines two specific depths at which the Young's modulus transitions to higher values: 150 m and 400 m. While in Martin (2007) the first depth (15 m) is interpreted as that at which open fracture sets in the rock mass are closed by the increased pressure, the second value (400 m), albeit necessary to fit measured data, is less intuitive and is not properly explained. We nevertheless applied the same depth dependency of the Young's modulus in our model and speculate that an overall increase in rock mass quality with depth could be justified. It should be noted that our model uses a third transition in the Young's modulus at a depth of 600 m. This corresponds to the maximum depth of the Martin (2007) stress model and in order to maintain a realistic distribution of Young's modulus with increasing depth a third transition was required.

In Chapter 3.1, we discussed some of the results of the Complete Site Investigation, which aimed, among other things, at defining the in-situ stress conditions at the Forsmark site. As previously mentioned, stress measurement campaigns yielded somewhat ambiguous results, with very different potential stress gradients (and stress regimes) fitting to different sets of measured data. If the homogeneity of the rock mass in terms of material parameters is indeed somewhat overestimated, as discussed above, the large variability encountered in the stress measurements could be to a certain extent justified. Moreover, as also pointed out in both Martin (2007) and Ask et al. (2007), several key issues are associated with the stress measurement campaign in Forsmark that could have resulted in poor data quality and large uncertainties in the derived stress gradients.

While our proposed model presents a very good fit to the stress regime from Martin (2007), we are fully aware of the intrinsic uncertainty that the original model carries: in the absence of better quality (and less variable) stress measurements, our modelling cannot reduce the risk that none of the originally proposed models for the Forsmark site (neither Martin, 2007 nor Ask et al., 2007) is in fact a realistic representation of the actual in-situ stress in the area.

In this sense, a source of uncertainty in the accuracy of the Martin (2007) model is the somewhat arbitrary change in Young's modulus at 400 m. This decision is not geologically justified in Martin (2007), but, in order to fit the change in stress gradients observed therein, it was necessary to implement the same depth-dependent variation in the Young's modulus within our model. Another cause of concern is the absence of stress measurements below a certain depth (ca. 700 m, although the majority of the measurements were actually performed within the first 500 m).

Evidently, all extrapolations of the stress gradients at greater depths (both in Martin, 2007 and in the currently proposed model) carry an intrinsic uncertainty that cannot be resolved with the current dataset of measured values. Specifically, the modelled stress we propose (while producing stress gradients that fall within the uncertainty envelopes defined by Martin, 2007) is characterised by a divergence of the Sh component (and to a lesser extent of the SH component) from the Martin (2007) gradients at depths greater than ca. 800 m. It should be noted, however, that values for the Young's modulus of the rock mass are given in Martin (2007) only down to a depth of 600 m, and the extrapolation of his stress curves to larger depths is purely linear. Our model, on the other hand, defines a maximum value for the Young's modulus (in both SH and Sh directions) at 2,200 m that is derived from modelling stage 2.3 (Glamheden et al., 2008). While this value is not tested for the large depth in question, we argue whichever extrapolation is applied below the maximum measurement depth (i.e. ca. 700 m) is bound to be characterised by a large degree of uncertainty.

Despite the fact that we aimed at modelling the stress field proposed by Martin (2007), any other proposed stress field (Gipper et al., 2015 and Ask et al., 2007) shows an overall deviation from the measured stress data, which based on our modelling cannot be explained by the perturbations produced by the fault zones alone (see Chapter 5.2). A possible explanation for the variations in the stress measurements might be given by the inhomogeneity of elastic properties. Specifically, the Young's modulus according to laboratory measurements can be assumed to vary on average up to 10% (e.g. Glamheden et al., 2007b, Glamheden et al., 2008). We therefore investigate the influence of the variation in Young's modulus and Poisson's ratio in an equivalent model without faults. The remaining parameters and boundary conditions are not changed.

Figure 21 shows the influence of randomly distributed Young's modulus and Poisson's ratio that both vary by ±10% around the values given in Chapter 3.2.1 for the Poisson's ratio (i.e. 0.3) and Chapter 5.1 for the calibrated depth- and direction-dependent Youngs modulus. The spread in stress values increases with depth to a maximum of about 15 MPa and is within the range of error envelopes proposed by Martin (2007) for the horizontal stresses.

The hereby built-in heterogeneity of rock mass parameters might provide an alternative explanation for the variations in stress measurements. Moreover, it highlights the possibility that the stress measurement data is influenced by locally varying rock properties and to a lesser extent by the existence of fault zones. The obtained stress values are roughly in the range of stress variability observed for overcoring stress measurements (compare Figure 1).

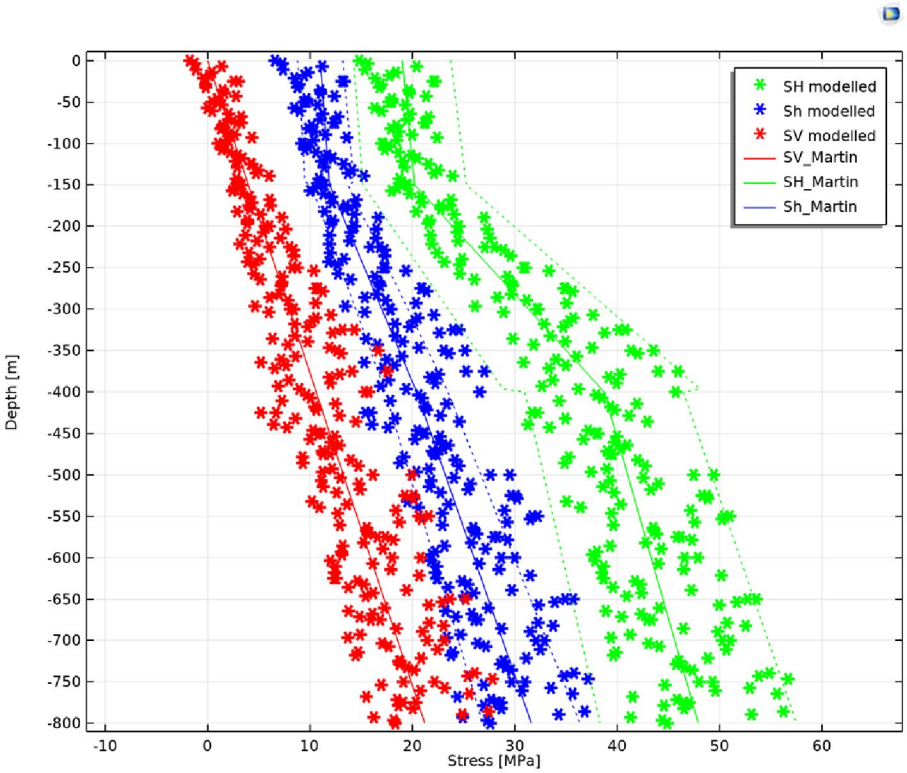

Figure 21 Change in the stresses for randomly distributed Poisson's ratio and Young's modulus.

7.3 Recommendations

Discrete faults seem to play a minor role in the current stress field in contrast to the spatial and heterogeneous distribution of rock properties. Research should be conducted on the spatial distribution and the range of rock properties so that calibrated distribution functions can be derived to populate the subsurface not with constant rock property values but with distribution functions that are based on spatial information or calibration. This might better address the uncertainties in the measured stresses than trying to approximate homogenized gradients not accurately describing the scatter of measured values. The performed modeling highlights the influence of elastic parameters on the stress field and shows how an assumption of a heterogeneous Young's modulus and Poisson's ratio of ±10% could describe the spread in the range of the most-likely stress field.

Hence, upcoming work could improve the capabilities of the model at hand by deriving spatial distribution function of elastic properties that are calibrated against the stress field measurements per well.

8 References

Ask, D., Cornet, F. & Fontbonne, F. (2007). Forsmark site investigation - Stress measurements with hydraulic methods in boreholes KFM07A, KFM07C, KFM08A, KFM09A and KFM09B. *P-07-206*.

Backers, T., Meier, T., Gipper, P. & Stephansson, O. (2014). Technical Note. Rock Mechanics - Confidence of SKB's models for predicting the occurrence of spalling – Main Review Phase. *SSM 2014:10*.

Bandis, S. C., Lumsden, A. C., Barton, N. R. (1983). Fundamentals of rock joint deformation. In International Journal of Rock Mechanics and Mining Sciences & Geomechanics Abstracts, Volume 20, Issue 6, 249-268, ISSN 0148-9062.

Gipper, P., Backers, T., & Lanaro, F. (2015, October). Re-evaluation of the in situ stress field at Forsmark, Sweden. In *ISRM Regional Symposium-EUROCK 2015*. OnePetro.

Glamheden, R., Maersk Hansen, L., Fredriksson, A., Bergkvist, L., Markström, I. & Elfström, M. (2007a). Mechanical modelling of the Singö deformation zone. Site descriptive modelling Forsmark stage 2.1. *SKB R-07-06.*

Glamheden, R., Fredriksson, A., Röshoff, K., Karlsson, J., Hakami, H. & Christiansson, R. (2007b). Rock mechanics Forsmark. Site descriptive modelling Forsmark stage 2.2. *SKB R-07-31.*

Glamheden, R., Lanaro, F., Karlsson, J., Lindberg, U., Wrafter, J., Hakami, H. & Johansson, M. (2008). Rock mechanics Forsmark. Modelling stage 2.3. Complementary analysis and verification of the rock mechanics model. *SKB R-08-66.*

Hökmark, H., Lönnqvist, M. and Fälth, B., 2010. THM-issues in repository rock. Thermal, mechanical, thermo-mechanical and hydro-mechanical evolution of the rock at the Forsmark and Laxemar sites. Technical report TR-10-23

Kulhawy, F. H. (1975). Stress deformation properties of rock and rock discontinuities. In Engineering Geology, Volume 9, Issue 4, 327-350,ISSN 0013-7952.

Martin, C. D. (2007). Quantifying in situ stress magnitudes and orientations for Forsmark Forsmark stage 2.2. *R-07-26.*

SKB TR-10-52. Data report for the safety assessment SR-Site. December 2010 (Updated 2014-01).

Stephens M. B., Simeonov A., 2015. Description of deformation zone model version 2.3, Forsmark. *SKB R-14-28.*

Zangerl C, Evans K F, Eberhardt E, Loew S, 2008. Normal stiffness of fractures in granitic rock: a compilation of laboratory and in-situ experiments. International Journal of Rock Mechanics and Mining Sciences 45, 1500–1507.

9 Appendix A

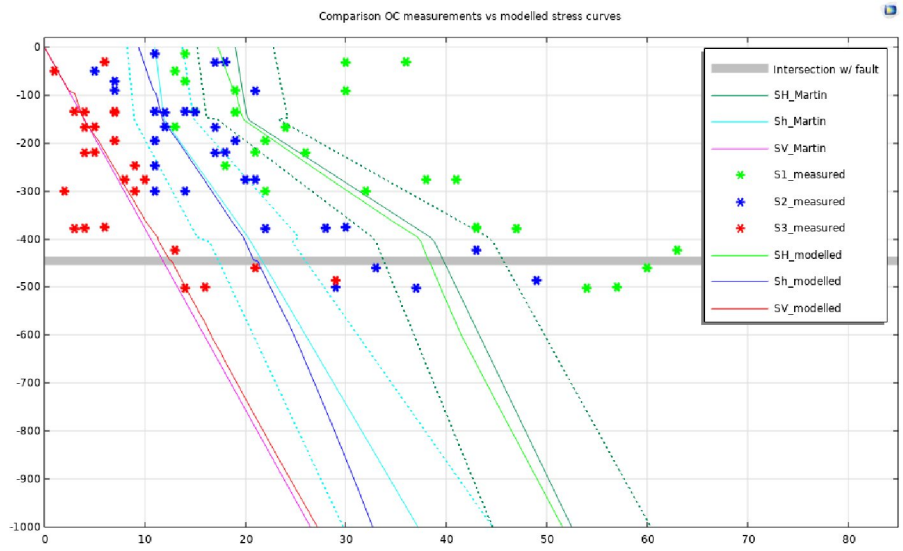

Figure A1 Comparison of the overcoring measurements collected in the DBT-1 borehole (shown as asterisks) and the stress curves modelled with k_n=1 GPa/m and k_s=0.1 GPa/m. The stress curves proposed by Martin (2007) are also shown (including the uncertainty envelopes, as stippled lines).

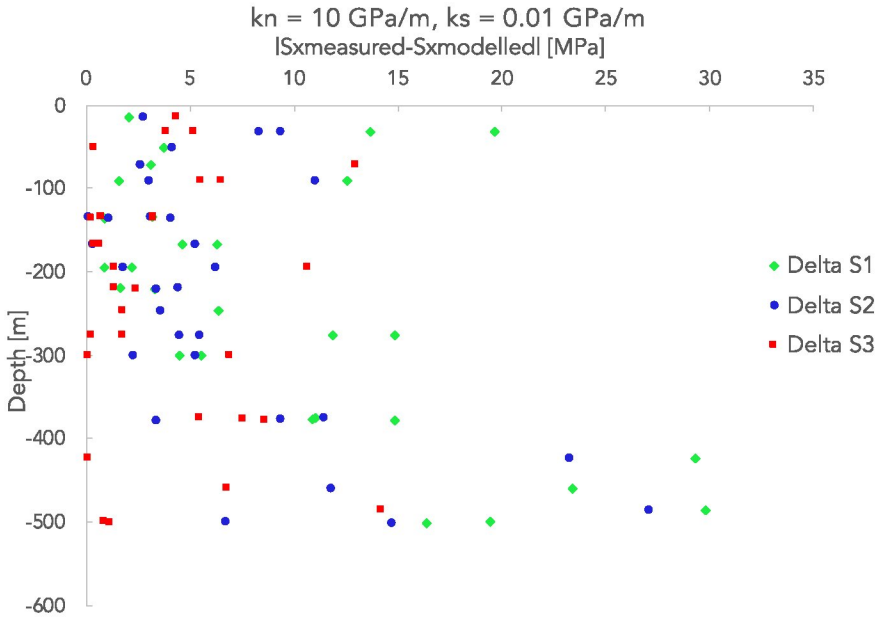

Figure A2 Difference between measured and modelled stress magnitudes for k_n=1 GPa/m and k_s=0.1 GPa/m plotted against depth. All three principal stresses are represented in the graph, in different colours.

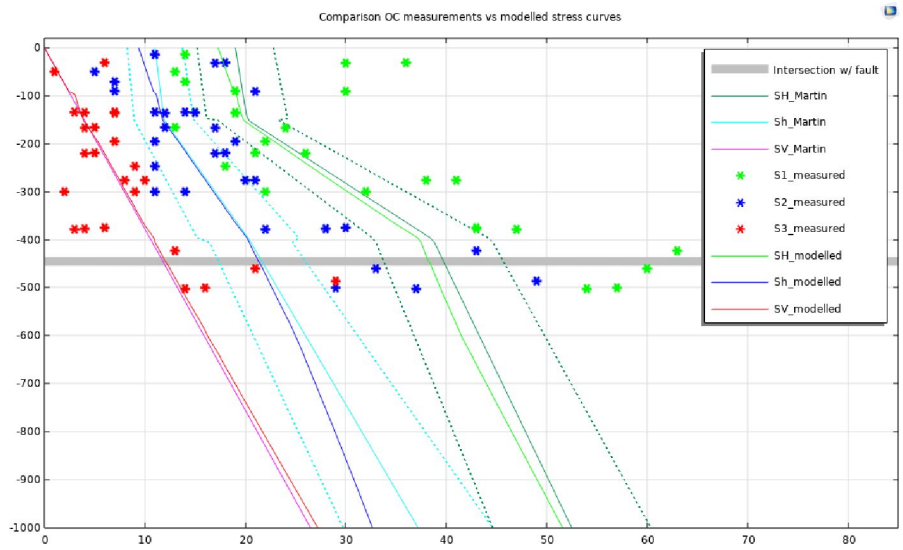

Figure A3 Comparison of the overcoring measurements collected in the DBT-1 borehole (shown as asterisks) and the stress curves modelled with k_n=10 GPa/m and k_s=1 GPa/m. The stress curves proposed by Martin (2007) are also shown (including the uncertainty envelopes, as stippled lines).

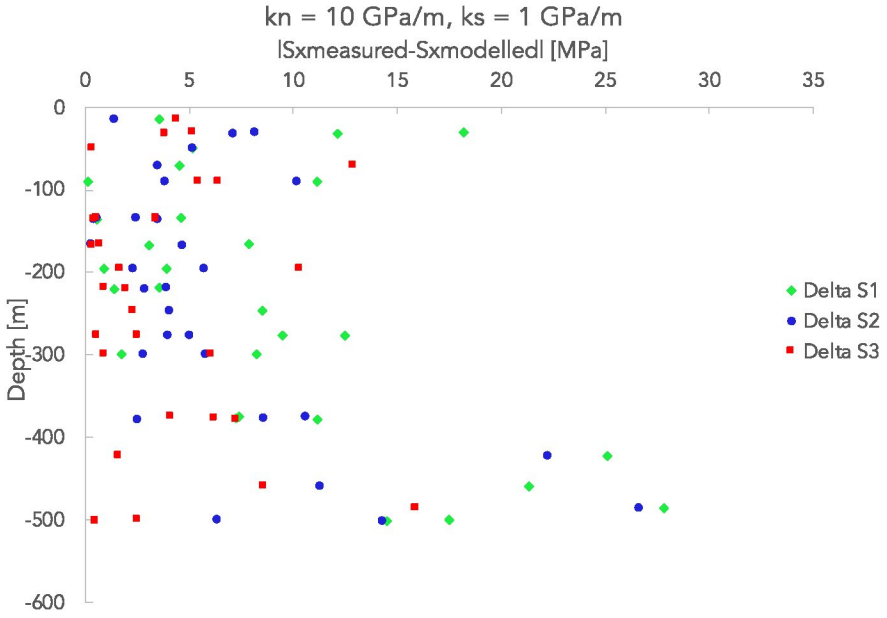

Figure A4 Difference between measured and modelled stress magnitudes for k_n=10 GPa/m and k_s=1 GPa/m plotted against depth. All three principal stresses are represented in the graph, in different colours.

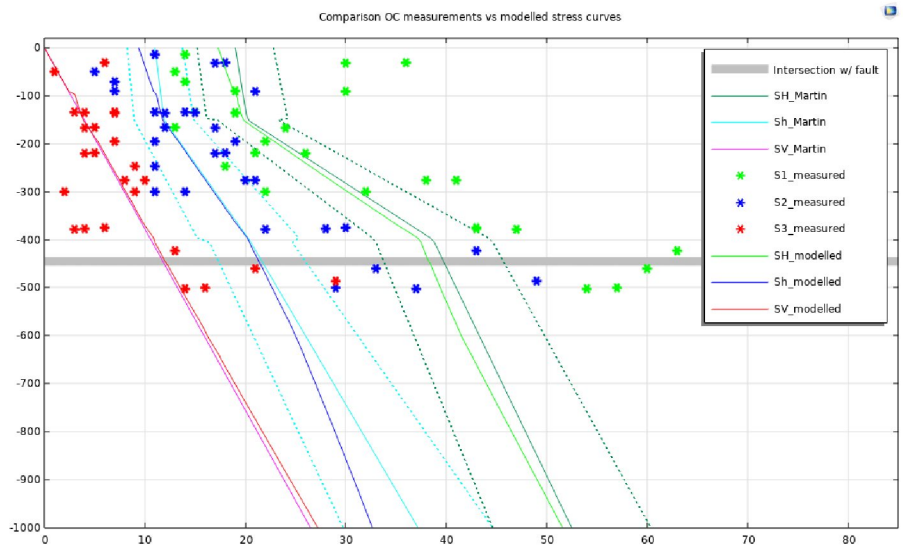

Figure A5 Comparison of the overcoring measurements collected in the DBT-1 borehole (shown as asterisks) and the stress curves modelled with k_n=20 GPa/m and k_s=2 GPa/m. The stress curves proposed by Martin (2007) are also shown (including the uncertainty envelopes, as stippled lines).

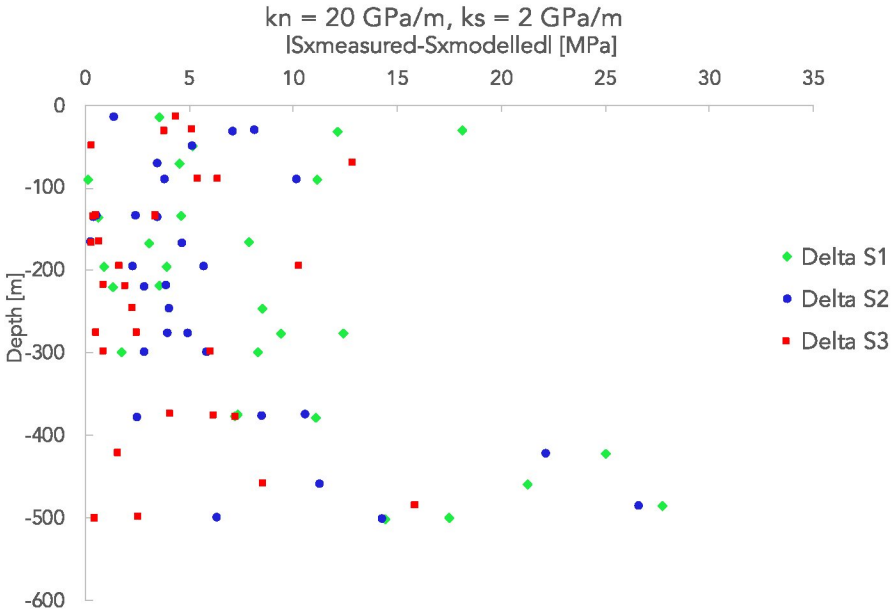

Figure A6 Difference between measured and modelled stress magnitudes for k_n=20 GPa/m and k_s=2 GPa/m plotted against depth. All three principal stresses are represented in the graph, in different colours.

10 Appendix B

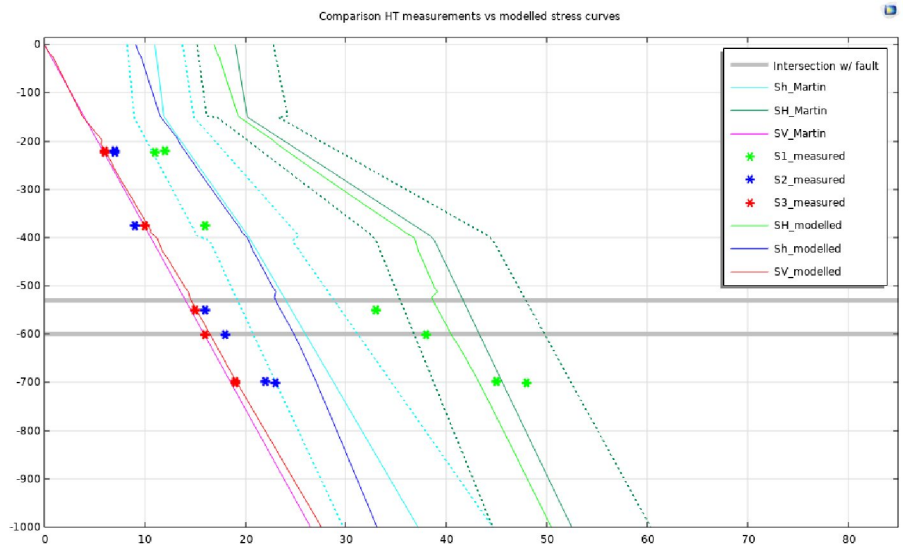

Figure B1 Comparison of the hydraulic test measurements collected in the KFM02A borehole (shown as asterisks) and the stress curves modelled with k_n=10 GPa/m and k_s=1 GPa/m. The stress curves proposed by Martin (2007) are also shown (including the uncertainty envelopes, as stippled lines).

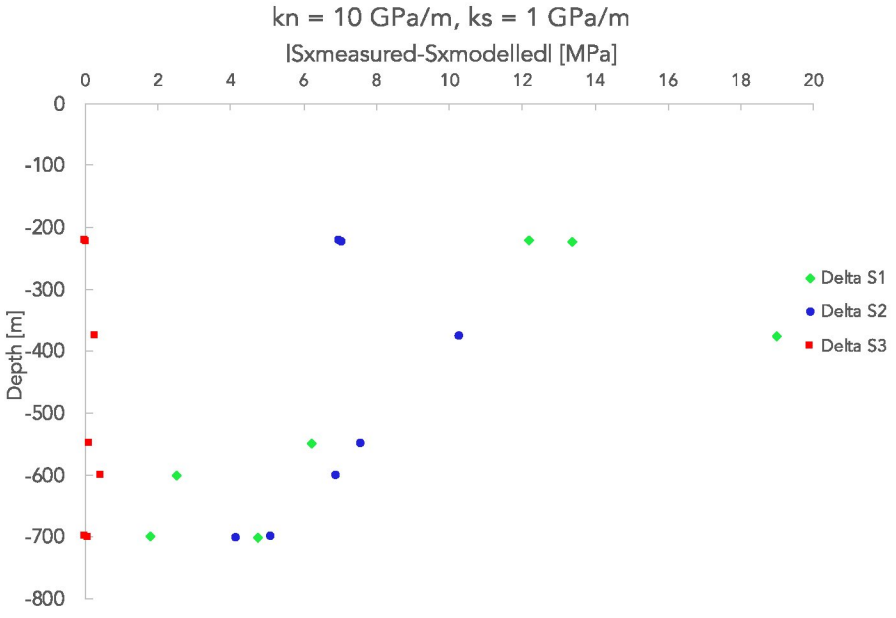

Figure B2 Difference between measured and modelled stress magnitudes for k_n=10 GPa/m and k_s=1 GPa/m plotted against depth. All three principal stresses are represented in the graph, in different colours.

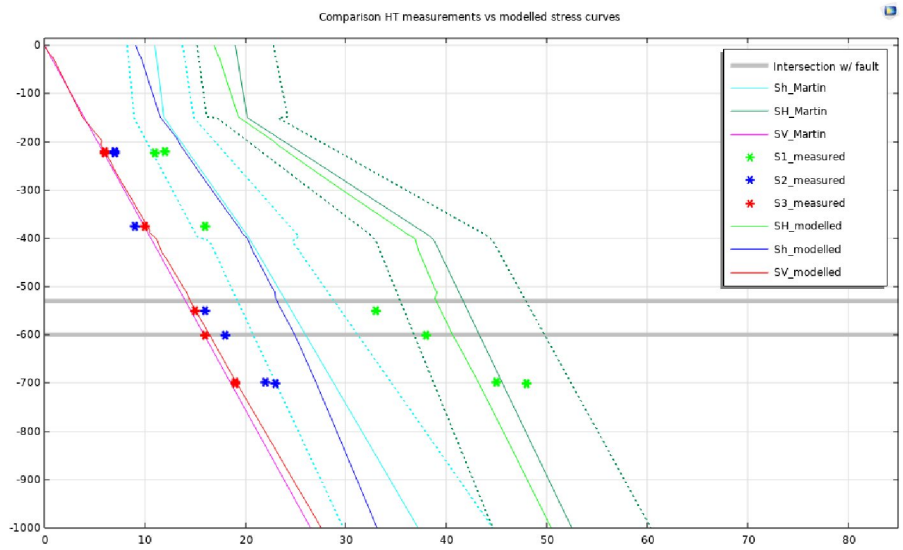

Figure B3 Comparison of the hydraulic test measurements collected in the KFM02A borehole (shown as asterisks) and the stress curves modelled with k_n=20 GPa/m and k_s=2 GPa/m. The stress curves proposed by Martin (2007) are also shown (including the uncertainty envelopes, as stippled lines).

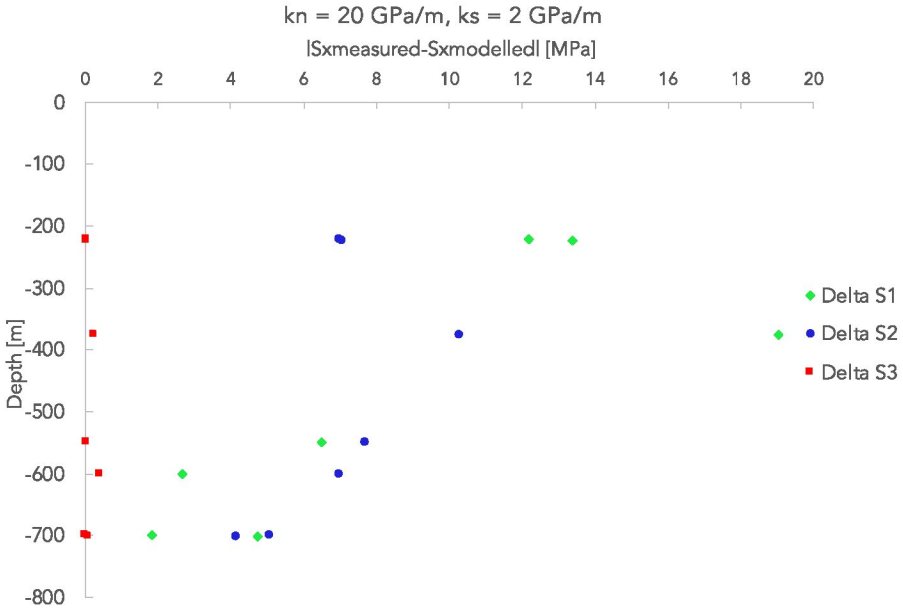

Figure B4 Difference between measured and modelled stress magnitudes for k_n=20 GPa/m and k_s=2 GPa/m plotted against depth. All three principal stresses are represented in the graph, in different colours.

The Swedish Radiation Safety Authority (SSM) works proactively and preventively with nuclear safety, radiation protection, nuclear security, and nuclear non-proliferation to protect people and the environment from the harmful effects of radiation, now and in the future.

You can download our publications from www.stralsakerhetsmyndigheten.se/en/publications. If you need alternative formats such as easy-to-read, Braille or Daisy, contact us by email at registrator@ssm.se.

Strålsäkerhetsmyndigheten
SE-171 16 Stockholm
+46 (0) 8-799 40 00
www.stralsakerhetsmyndigheten.se
registrator@ssm.se

©Strålsäkerhetsmyndigheten

E-print AB, 2024